AGU PUBLICATIONS

JGR

Journal of Geophysical Research: Oceans

RESEARCH ARTICLE

10.1002/2017JC012791

The Importance of Freshwater to Spatial Variability of Aragonite Saturation State in the Gulf of Alaska

Samantha A. Siedlecki[1], Darren J. Pilcher[1,2], Albert J. Hermann[1,2], Ken Coyle[3], and Jeremy Mathis[4]

[1]Joint Institute for the Study of the Atmosphere and Ocean, University of Washington, Seattle, WA, USA, [2]NOAA Pacific Marine Environmental Laboratory, NOAA, Seattle, WA, USA, [3]College of Fisheries and Ocean Sciences, University of Alaska Fairbanks, Fairbanks, AK, USA, [4]NOAA Headquarters, Silver Spring, MD, USA

Key Points:
- Alkalinity of glacial meltwater is an important driver of the variability in aragonite saturation state of the nearshore waters, and is fairly unconstrained
- Local winds, biological processes, and freshwater forcing all contribute to the spatial distribution of aragonite saturation state in the Gulf of Alaska

Correspondence to:
S. A. Siedlecki,
siedlesa@uw.edu

Citation:
Siedlecki, S. A., Pilcher, D. J., Hermann, A. J., Coyle, K., & Mathis, J. (2017). The importance of freshwater to spatial variability of aragonite saturation state in the Gulf of Alaska. *Journal of Geophysical Research: Oceans*, *122*, 8482–8502. https://doi.org/10.1002/2017JC012791

Received 10 FEB 2017
Accepted 6 SEP 2017
Accepted article online 26 SEP 2017
Published online 7 NOV 2017

Abstract High-latitude and subpolar regions like the Gulf of Alaska (GOA) are more vulnerable than equatorial regions to rising carbon dioxide (CO_2) levels, in part due to local processes that amplify the global signal. Recent field observations have shown that the shelf of the GOA is currently experiencing seasonal corrosive events (carbonate mineral saturation states Ω, $\Omega < 1$), including suppressed Ω in response to ocean acidification as well as local processes like increased low-alkalinity glacial meltwater discharge. While the glacial discharge mainly influences the inner shelf, on the outer shelf, upwelling brings corrosive waters from the deep GOA. In this work, we develop a high-resolution model for carbon dynamics in the GOA, identify regions of high variability of Ω, and test the sensitivity of those regions to changes in the chemistry of glacial meltwater discharge. Results indicate the importance of this climatically sensitive and relatively unconstrained regional freshwater forcing for Ω variability in the nearshore. The increase was nearly linear at 0.002 Ω per 100 μmol/kg increase in alkalinity in the freshwater runoff. We find that the local winds, biological processes, and freshwater forcing all contribute to the spatial distribution of Ω and identify which of these three is highly correlated to the variability in Ω. Given that the timing and magnitude of these processes will likely change during the next few decades, it is critical to elucidate the effect of local processes on the background ocean acidification signal using robust models, such as the one described here.

1. Introduction

Rising carbon dioxide (CO_2) levels in the atmosphere are driving increased uptake of CO_2 by the ocean, thereby causing the marine environment to become more acidic and carbonate ion concentration ($[CO_3^{2-}]$) to decline. Consequently, saturation states of carbonate biominerals (Ω) essential for shell-forming organisms are also declining (Caldeira & Wickett, 2003, 2005; Doney et al., 2009; Feely et al., 2004; Orr et al., 2005). Ω is defined as the ratio $[Ca^{2+}][CO_3^{2-}]/K^*sp$, where K*sp is the temperature, salinity, and pressure-dependent apparent solubility product for the aragonite or calcite carbonate mineral phase. Precipitation of carbonate biominerals is possible when $\Omega > 1$, with higher values corresponding to conditions more energetically favorable for precipitation (Fabry et al., 2008; Feely et al., 2004; Orr et al., 2005). The intrusion of atmospheric CO_2 and its associated impacts on ocean carbon chemistry has been termed "ocean acidification" (OA), and it could have far-reaching consequences for pelagic and benthic calcifying organisms, particularly in the cold, highly productive coastal waters of the Gulf of Alaska (GOA), due to the higher capacity of cold waters to absorb CO_2 (Mathis et al., 2015). However, the intrusion of atmospheric CO_2 is not the only mechanism that can reduce pH or Ω in the surface ocean; local processes that drive variability at the regional level also play a role in the spatial variability of Ω in association with the global changes associated with anthropogenic CO_2.

Recent field observations (Evans et al., 2013, 2015) have shown that the inner and middle shelf of the GOA currently experiences seasonal manifestations of corrosive events ($\Omega < 1$), including decreased pH and suppressed Ω in response to rising CO_2 levels and increased discharge of low-alkalinity, glacial meltwater (Evans et al., 2014; Reisdorph & Mathis, 2015). While the glacial discharge mainly influences water on the inner shelf, upwelling brings nutrient and CO_2-rich waters that are undersaturated in the calcium carbonate mineral aragonite from the deep GOA onto the outer shelf (Evans et al., 2013). Throughout most of the year, regional winds generate a downwelling circulation, which keeps deeper water offshore. In summer,

however, these winds relax, which allows undersaturated waters to penetrate the inner shelf, causing the saturation horizon for aragonite to become as shallow as 75 m (Evans et al., 2013). In addition, remineralization of organic matter at depth may further decrease the pH and Ω in the bottom waters, as this is the case in other regions (Feely et al., 2016; Siedlecki et al., 2015). Most of the characterization of seasonal variability of corrosive conditions in the region has focused on the northern GOA shelf and Prince William Sound, which has limited our ability to project basin-wide changes due to OA. Some recent observations (J. Cross, personal communication, 2016) include more of the eastern GOA, where the processes responsible for Ω variability in the eastern GOA (e.g., freshwater discharge, the degree of downwelling, and local biological processes) appear to be the same combination, although the relative importance of each is probably different. The question is: how important is each process within different regions of the GOA?

These processes are projected to change as the global climate changes over the next few decades. Freshwater peak forcing is expected to shift to greater fall discharge under IPCC Scenario RCP 8.5 conditions (Hill et al., 2015). Currently, 47% of the total freshwater discharge into the GOA is derived from glaciers and icefields, with 7%–10% attributed to glacier volume loss (Hill et al., 2015; Neal et al., 2010). Those freshwater drivers are expected to change to less ice melt, more snowmelt, more rainfall, a change in the timing of the discharge, and a change from tidewater glaciers that melt directly into the ocean to mountainous glaciers that feed proglacial streams prior to delivery to the ocean (Larsen et al., 2015). All of these changes have implications for the total alkalinity (TA) of the freshwater contributions to the GOA, which can influence Ω. The more interaction that freshwater has with bedrock and glacial sediments, the higher the TA is expected to be (Anderson et al., 2000; Brown, 2002). Runoff delivered from tidewater glaciers generally contains lower TA (400–700 μmol kg^{-1}) when compared to runoff delivered from proglacial streams (1,200–1,300 μmol kg^{-1}; Alkire et al., 2015; Anderson et al., 2000; Fransson et al., 2015). In addition to changes in freshwater chemistry and magnitude, the wind forcing is expected to become less downwelling favorable (Yin, 2005), while productivity of the basin is expected to decline in the future (Polovina et al., 2010). Each of these processes will alter the spatial expression of carbon dynamics in the GOA, which will impact the habitats of organisms sensitive to pH, Ω, CO_2, or CO_3.

The GOA ecosystems and their associated fisheries are some of the most productive and lucrative in the world, and are composed of many organisms (oysters, mussels, clams, geoducks, crabs, finfish, and pteropods) sensitive to Ω or pH and the changes associated with OA (Mathis et al., 2015). While all of these organisms are important for the GOA ecosystem and ecosystem services, they occupy very different regions of the marine environment, which are subject to different mechanisms governing that region's variability in Ω.

In this work, we develop a well-validated, high-resolution model for Ω, pH, and carbon variability in the GOA, identify regions of high variability, and test the sensitivity of those regions to changes in the chemistry of glacial discharge. In our model calculations for 2009, we find that the chemistry of the freshwater forcing is an important driver for the regions near the land at the surface. The local winds, biological processes, and freshwater forcing all contribute to generating the spatial distribution of Ω in the GOA. Local biological processes are the dominant control on spatial variability of surface Ω in offshore waters of the region, while freshwater forcing is the dominant control in the nearshore waters. The depth of the Ω horizon is correlated with local biological processes in the central GOA and the salinity forcing in the western and eastern GOA.

1.1. Regional Oceanography

The Alaska Coastal Current (ACC) is a buoyancy-driven westward flowing current within 40 km of the coast. Approximately two thirds of the along-shelf (baroclinic) transport is carried within the ACC, making it the most prominent circulation feature of the GOA shelf (Figure 1). The current originates on the British Columbian shelf (Royer, 1998) and flows northward through the passages of southeast Alaska, before entering the Bering Sea through Unimak Pass in the western GOA (Schumacher & Reed, 1980; Stabeno et al., 2002; Weingartner et al., 2005) (Figure 1). It thus spans an alongshore distance of ∼2,000 km, making it one of the longest (albeit not continuous; see Stabeno et al., 2002) coastal currents in the global ocean.

A portion of the ACC flows through Prince William Sound (Figure 1; Niebauer et al., 1994; Royer et al., 1990; Vaughan et al., 2001) and, thus affects the heat, salt, nutrient, and carbon budgets of the sound and its adjacent bays (Gay & Vaughan, 2001). This narrow (∼40 km), swift, year-round flow is maintained by the integrated forcing of winds and freshwater discharge with seasonally high rates of glacier runoff (Evans et al., 2014). Both the winds and the discharge vary seasonally, although not in-phase with one another: discharge

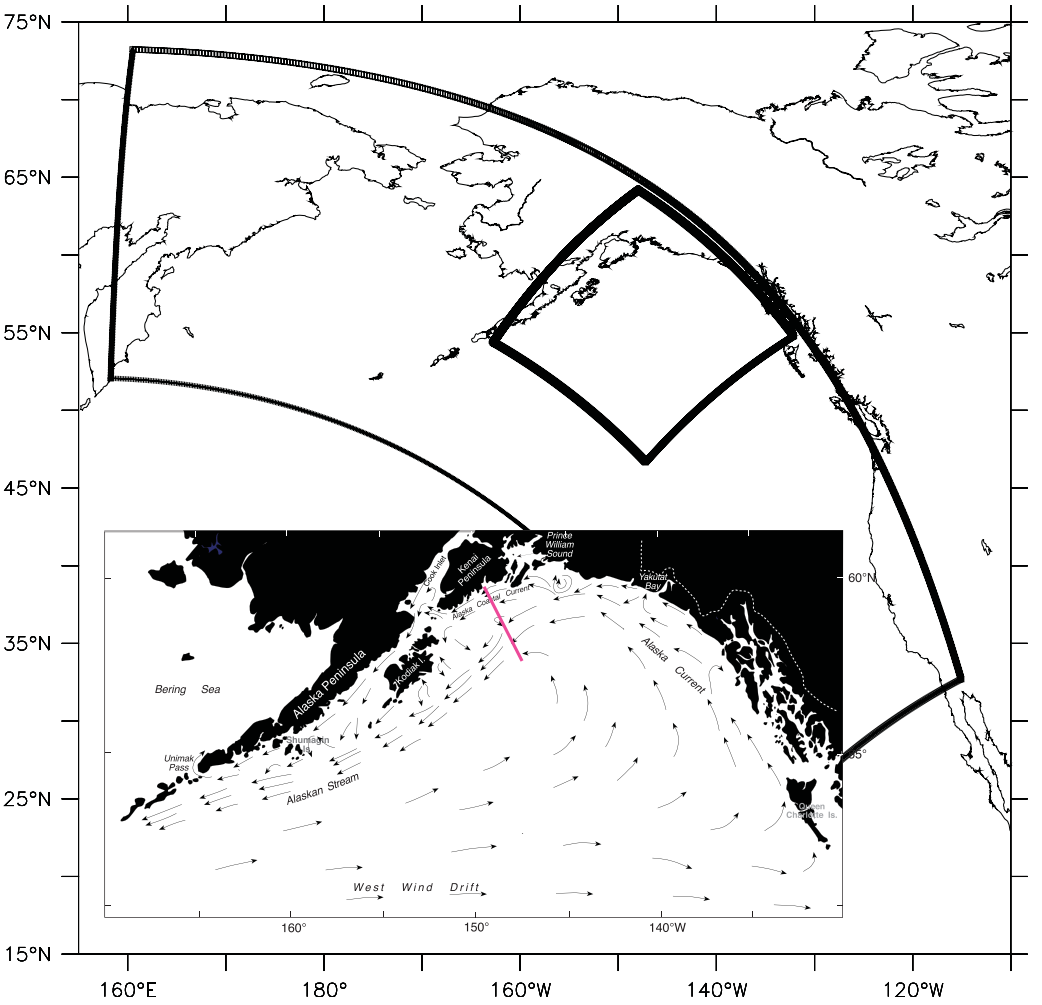

Figure 1. Model region after Hinckley et al. (2009). Diagram showing the nested model grids from Hermann et al. (2009b). Large grid is from the NEP model and the small grid is the GOA model. Insert is the coastal GOA showing major current systems as well as the location of the Seward Line in pink.

is a maximum in fall and the westward (downwelling-favorable) winds are strongest in winter. The winds in the winter mix the shelf down to 100–200 m. The runoff contribution to the shelf is massive ($\sim$24,000 m^3 s^{-1}; or 20% greater than the Mississippi River discharge) and in combination with wind forcing affects shelf dynamics, stratification, nutrient loads, and carbon biogeochemistry. The principal drivers of this shelf ecosystem also vary substantially at interannual and longer time scales (Hermann et al., 2016; Royer, 2005; Stabeno et al., 2004; Weingartner et al., 2005), although the variability is poorly understood.

Changes in both the amount of daily light and the depth of mixing initiate an extensive phytoplankton bloom in spring (late April to early June). Chlorophyll *a* concentrations can vary from <1 μg L^{-1} in winter to >30 μg L^{-1} during the spring bloom when surface nutrients are rapidly depleted (Napp et al., 1996; Strom et al., 2006) and dissolved inorganic carbon (DIC) concentrations are drawn down. The northern shelf is spatially heterogeneous and can be extremely productive, with annual rates ranging from $\sim$140 to 300 g C m^{-2} compared to 48 g C m^{-2} at Ocean Station Papa (Sambrotto & Lorenzen, 1987). The highly productive nature of the shelf is somewhat surprising because of consistent downwelling throughout most of the year. A high rate of productivity is associated with the vertical mixing of nutrient-rich water from the GOA or eddies from the offshore region (Hermann et al., 2009b), due to the low nitrate load in freshwater sources to the inner shelf (i.e., glacial). Iron sources from coastal runoff also drive productivity in the region; in a general sense, the productivity is due to the confluence of high nitrate waters from offshore with high iron

waters from inshore (Coyle et al., 2012; Stabeno et al., 2004; Wu et al., 2009). There is significant interannual variability in the magnitude and timing of these blooms, which are dependent on factors such as the extent of cloud cover, the intensity of stratification, and grazing (Napp et al., 1996).

As the bloom progresses, large standing crops of phytoplankton can build up over the inner shelf in summer and dense chlorophyll *a* concentrations usually appear briefly in surface waters (Brickley & Thomas, 2004; Waite & Mueter, 2013), although subsurface chlorophyll *a* layers can persist throughout summer. Nitrate and silicate concentrations decline rapidly, and low levels of primary production are sustained through the summer by nutrient recycling in the photic zone, by nitrogen fixation, and by localized upwelling and turbulent mixing (Hermann et al., 2009b; Sambrotto & Lorenzen, 1987). During the periods of relaxed coastal downwelling in summer (more so in some years than in others), the intrusion of subsurface slope water onto the shelf provides a mechanism for nutrient enrichment in the bottom waters. In winter, cooling and enhanced winds weaken stratification, causing mixing all the way to the bottom of the inner shelf and entraining high concentrations of nutrients into surface waters.

All of these observations suggest that the coastal environment and ACC is an important ocean pathway by which climate signals, dissolved and suspended materials, contaminants, and organisms are advected from the Gulf and into the Bering Sea (Figure 1). Natural variability in the marine carbon cycle must be quantified and its causes understood in order to comprehend and predict the response of the GOA marine ecosystem to natural or human-related perturbations, such as OA.

In this work, spatial variability of the surface Ω as well as the depth of the Ω saturation horizon is examined using a high-resolution regional model for the GOA. In section 2, the methods are outlined, including a description of the carbon model (section 2.2) and the model simulations (section 2.4). Section 3 summarizes the results, including model performance (section 3.1) and the results of the spatial correlations (section 3.4). In section 4, controls over spatial variability and potential changes in the future are discussed. Finally, section 5 summarizes the results. We find that spatial and temporal patterns of local winds, biological processes, and freshwater forcing all contribute to generating the spatial distribution of Ω in the GOA.

2. Methods

2.1. Physical Model Description

The high-resolution model used here is based on the Regional Ocean Modeling System (ROMS; Rutgers version 3) (Haidvogel et al., 2008; Shchepetkin & McWilliams, 2005) and is configured for the Gulf of Alaska as described in detail by Dobbins et al. (2009), Hermann et al. (2009b), and Coyle et al. (2012). The domain (Figure 1) extends from 48°N to 65°N with a horizontal resolution of 3 km and 42 vertical levels. The model is nested within a larger grid referred to as the Northeast Pacific model (NEP; Curchitser et al., 2005; Danielson et al., 2011; Hermann et al., 2009a). While the same physical model is used in both, the grid differs between the GOA model and the NEP model as indicated in Figure 1. Tidal dynamics (and the consequent tidal mixing) are included in both models. The model was initialized from a long-term continuous simulation that began in year 2000, which included all the model fields except for DIC and TA.

2.2. Biogeochemical Model Description

In this work, we couple the cycling of DIC and alkalinity to the existing ecosystem model framework (Figure 2). The nitrogen budget and planktonic nutrient cycling is described in detail by Coyle et al. (2012), along with additional evaluation of model performance. The ecosystem model has been used in a variety of studies in the GOA (Cheng et al., 2012; Coyle et al., 2012, 2013; Hermann et al., 2009a; Hinckley et al., 2009). The biogeochemical model consists of the following state variables: small phytoplankton (*PS*); large phytoplankton (*PL*); four different zooplankton—small microzooplankton (MZS), large microzooplankton (*MZL*), copepods (*C*), and Neocalanus (*NC*); and dissolved nutrients—nitrate (NO_3) and ammonia (NH_4), detritus (*D*), and iron (*Fe*). For simplicity in the equations that follow, the zooplankton (*Z*) and the phytoplankton (P) pools will be combined into a single *Z* or *P* reservoir. A list of variables and parameter values is given in Coyle et al. (2012, Table A2), and a simplified schematic of the state variables and their interactions with *DIC* and *TA* is illustrated in Figure 2. Respiration is termed "remineralization" in Figure. 2 and is represented in the model. Denitrification is ignored as the oxygen concentrations in the water column in the GOA remains high relative to other regions of the North Pacific and this model largely ignores sedimentary processes.

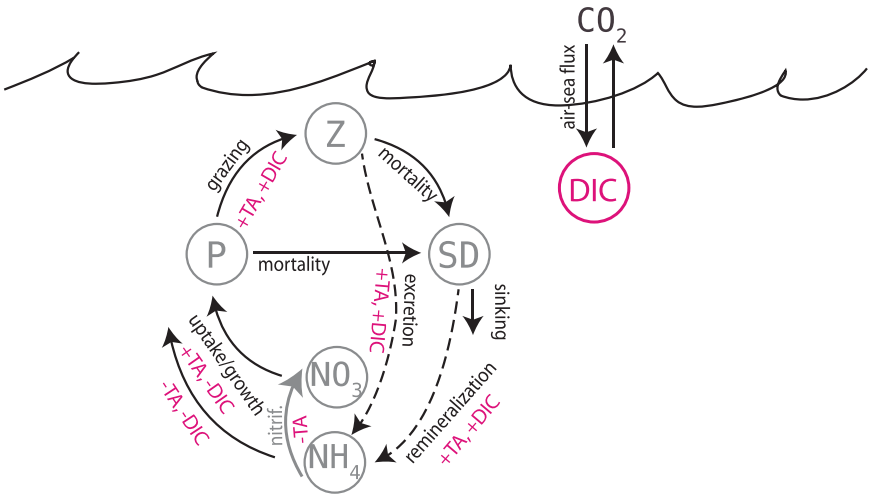

Figure 2. Cartoon of biogeochemical model for the GOA.

This assumption seems valid given the limited observations existing in the northern GOA indicate denitrification is negligible (Haines et al., 1981). The model is written in terms of reservoirs of carbon, and conversion to nitrogen (for *TA*) is made with the Redfield ratio (106:16; Sarmiento & Gruber, 2006). The time evolution of *DIC* and *TA* is calculated using a modification of the framework of Fennel et al. (2008) as implemented in ROMS v2.2 (see also schematic in Figure 2, and equations below) with modifications for ammonia cycling and freshwater conditions as outlined below. Definitions and units for all variables are given in Coyle et al. (2012, Table A2) and the governing equations for *DIC* are given here, and in the Appendix A (A1) in the same style as Coyle et al. (2012):

$$\frac{\partial DIC}{\partial t} = rD - \mu_i(E,N,Fe)P + resp(P) + G(P)Z + advection + diff \tag{1}$$

$$\left.\frac{\partial DIC}{\partial t}\right|_{bottom} = \frac{1}{\Delta z}\left(w_D \left.\frac{dD}{dz}\right|_{z=bottom}\right) \tag{2}$$

$$\left.\frac{\partial CO_2}{\partial t}\right|_{surface} = \frac{V_{CO2}}{\Delta z} * [CO_2]_{sol} * \left([CO_2]_{air} - [CO_2]|_{z=surface}\right) \tag{3}$$

where $V_{CO2} = 0.31u^2\left(\frac{Sc}{660}\right)^{-0.5}$, u is the wind speed at the surface, Sc is the Schmidt number from Wanninkhof (1992), and $[CO_2]_{sol}$ is the solubility of CO_2 computed using the formula from Weiss (1974). DIC is consumed by phytoplankton (P) growth (μ_i), which is light (E) and nutrient limited (N) and iron (Fe) limited, as described in Coyle et al. (2012), and is produced by respiration (*r, resp*) of detritus, phytoplankton, zooplankton, and grazing (G) of zooplankton. Air-sea exchange of CO_2 at the surface also affects the DIC concentration, with an invasion from the atmosphere increasing DIC and escape from the ocean to the atmosphere decreasing DIC. Each of these processes is a function of temperature as well. At the bottom, a Neumann boundary condition is assumed with a zero flux so no material leaves the domain vertically.

Alkalinity cycling is affected by many of the same biological and physical drivers as *DIC*, with the exception of air-sea gas exchange and the added process of nitrification. The governing equations and in the Appendix A (A2) in the same style as Coyle et al. (2012), for *TA* are:

$$\frac{\partial TA}{\partial t} = \mu_i(E,NO3,Fe)P - \mu_i(E,NH4,Fe)P + rD + resp(P) + G(P)Z - 2 * Nitrif + advection + diffusion \tag{4}$$

$$\left.\frac{\partial TA}{\partial t}\right|_{bottom} = \frac{1}{\Delta z}\left(w_D \left.\frac{dTA}{dz}\right|_{z=bottom}\right) \tag{5}$$

where *NO3* is the nitrate concentration, *NH4* is the ammonia concentration, z is depth, and *Nitrif* is nitrification. More information about these variables can be found in Coyle et al. (2012, Table A2). The uptake of nitrate versus ammonia by phytoplankton alters alkalinity differently after Brewer and Goldman (1976) and

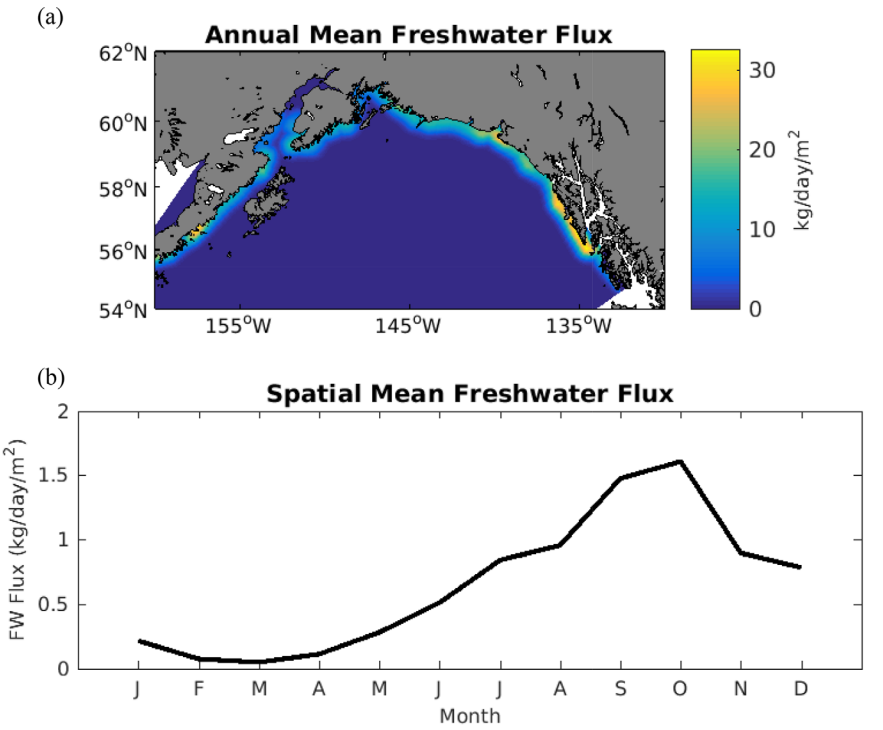

Figure 3. (a) Annual mean freshwater flux and (b) spatially averaged freshwater flux for 2009. The freshwater flux values have monthly time resolution.

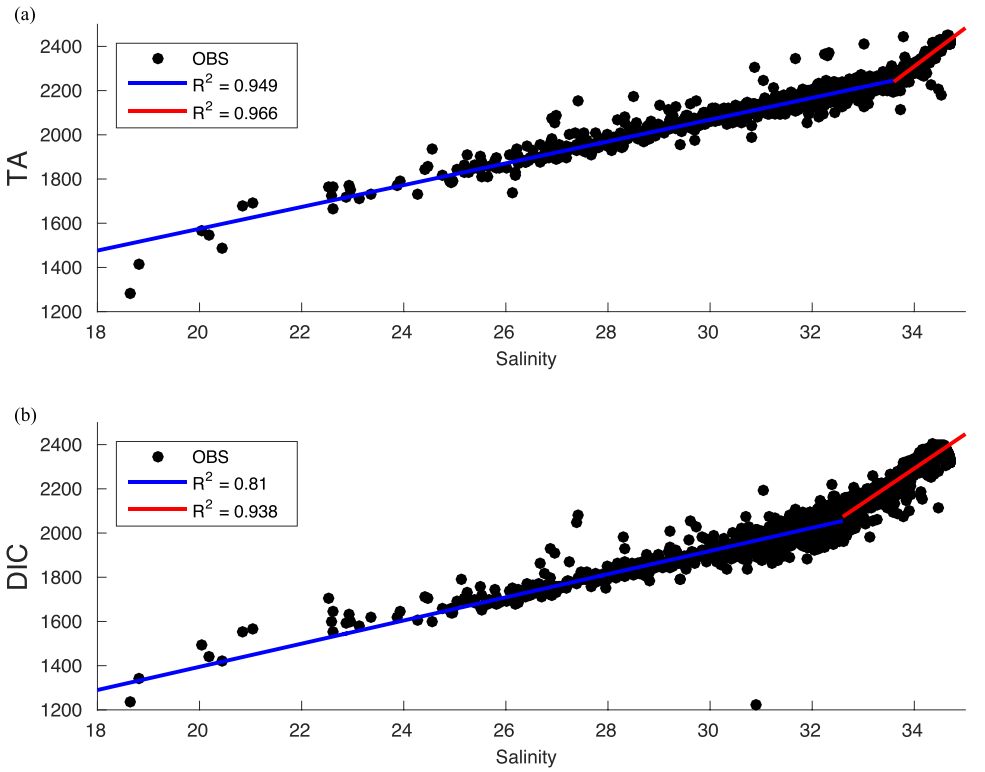

Figure 4. Observed values of (a) TA and (b) DIC plotted against salinity. Observed values are compiled from 2008 to 2012 Seward Line data, P16 (1991, 2006), and P17 (1993, 2001) cruise data. The two linear fits (blue and red lines) are calculated using a cutoff salinity value of 32.6 for DIC and 33.6 for TA.

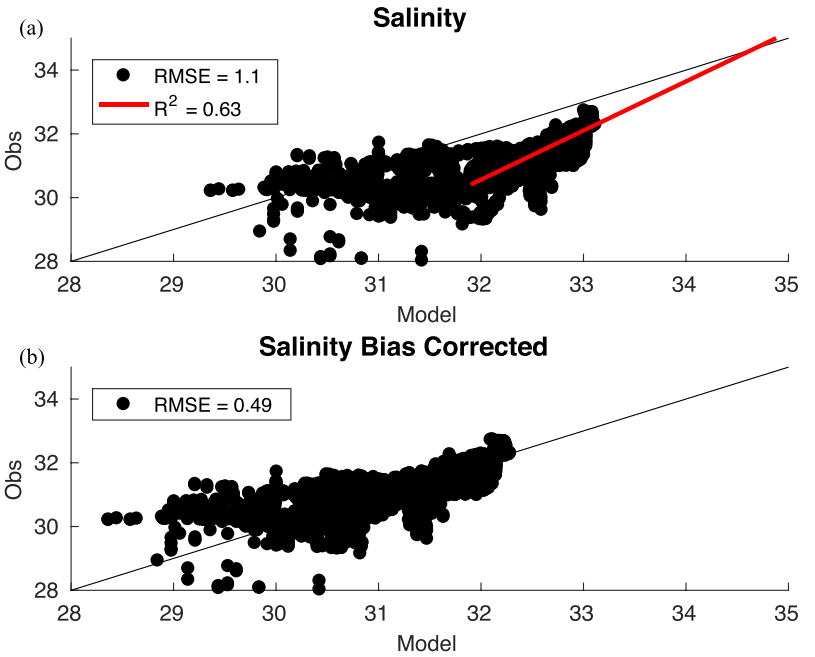

Figure 5. Observed salinity from the 2009 Coastal uwpCO$_2$ cruise compared to model salinity with a black 1:1 line for visual reference. (a) The model salinity bias and the linear fit used to correct model salinity values greater 31.9 (red line). (b) Model salinity after correcting for the salinity bias.

Goldman and Brewer (1980), as described in Zeebe and Wolf-Gladrow (2001). Alkalinity increases by one mole in response to the uptake of one mole of nitrate by phytoplankton because the uptake occurs simultaneously with the uptake of H+ and release of OH–. Conversely, the uptake of ammonia produces a decrease of alkalinity for the same reason (release of H+ and consumption of OH–) (Brewer & Goldman, 1976). Nitrification decreases alkalinity through the addition of H+ in the conversion to nitrate (Brewer & Goldman, 1976). Remineralization and grazing of organic material has the inverse effect on alkalinity.

2.3. Freshwater Forcing

Estimates of distributed freshwater input for the GOA come from monthly values of runoff integrated along the entire Alaskan coast, as derived by Royer (1982, and personal communication, 1994) from snowpack, precipitation, and temperature data. Additional point sources of runoff were derived from USGS river data. More details can be found in Dobbins et al. (2009) and Coyle et al. (2012). Our prior experience with the CGOA model indicated that for the distributed source, a simple application of all freshwater at the coastal boundary, while intuitively a more "realistic" application scheme, in practice results in excessive vertical stratification and horizontal penetration of a thin surface freshwater wedge much further out on the shelf than is observed (e.g., see Figure 14 of Dobbins et al., 2009). This artifact, believed due primarily to our limited resolution of shallow estuarine mixing in the CGOA, can be reduced by several methods, including: (1) artificially enhancing the salinity of the runoff (which violates salt conservation); (2) spreading the source waters over multiple grid points near the coast (effectively premixing the runoff in the cross-shelf direction, but otherwise permitting coastal currents to arise as an emergent property of the model dynamics). In the present work, we utilize the second method. Specifically, the cross-shelf pattern was set using an exponential taper based on squared distance from the coastline, with an *e*-folding distance of ~30 km (the typical width of the Alaska Coastal Current [ACC]). This supplies most of the runoff within ~4 grid points of the coastline, with decreasing input further out (and none beyond 30 km of the coastline). Independently, the climatology of Dai et al. (2009) was used to set the mean alongshore spatial pattern of the runoff. This fixed cross-shore/alongshore spatial pattern is then used to distribute the aforementioned total monthly runoff estimates for the CGOA, which are based on measured rainfall and temperature. The spatial pattern is normalized to ensure mass conservation, so that the total runoff is fully distributed over the CGOA during each month. The spatial pattern and a typical seasonal cycle for this forcing are illustrated in Figure 3.

Table 1
Tests for Alkalinity

Experiment name	TA concentration (μmol/kg)	Comparable systems	Reference
Low alkalinity	650	Amazon River, current CGOA inflow, tidewater glacial runoff	Devol and Hedges (2001) and Evans et al. (2014)
Intermediate	1,550	Arkansas and Ohio Rivers, Bench Glacier foreland	Stets et al. (2014) and Anderson et al. (2000)
High alkalinity	1,950	Yukon River	Cooper et al. (2008)

2.4. Boundary and Initial Conditions

The NEP specifies water entering the domain at the open boundaries. Biogeochemical boundary conditions were implemented using local empirical relationships with salinity for NO_3, DIC, and TA. Boundary and initial conditions for TA and DIC used observational data from the Northeast Pacific Global Ocean Ecosystems Dynamics (GLOBEC) Seward Line and from the repeat hydrography cruises P16N and P17N to calculate robust linear regressions between DIC, TA, and salinity (Figure 4):

$$S < 32.6 \;\; DIC = 52.4 * S + 346.5 \tag{6}$$

$$S > 32.6 \;\; DIC = 155.8 * S - 3,005.0 \tag{7}$$

$$S < 33.6 \;\; TA = 49.4 * S + 588.0 \tag{8}$$

$$S > 33.6 \;\; TA = 173.7 * S - 3,596.0 \tag{9}$$

where S represents the salinity. This regression is comparable to previous salinity linear regressions used for TA and DIC in the GOA (Evans et al., 2014, 2015). The TA and DIC distributions bend at slightly different

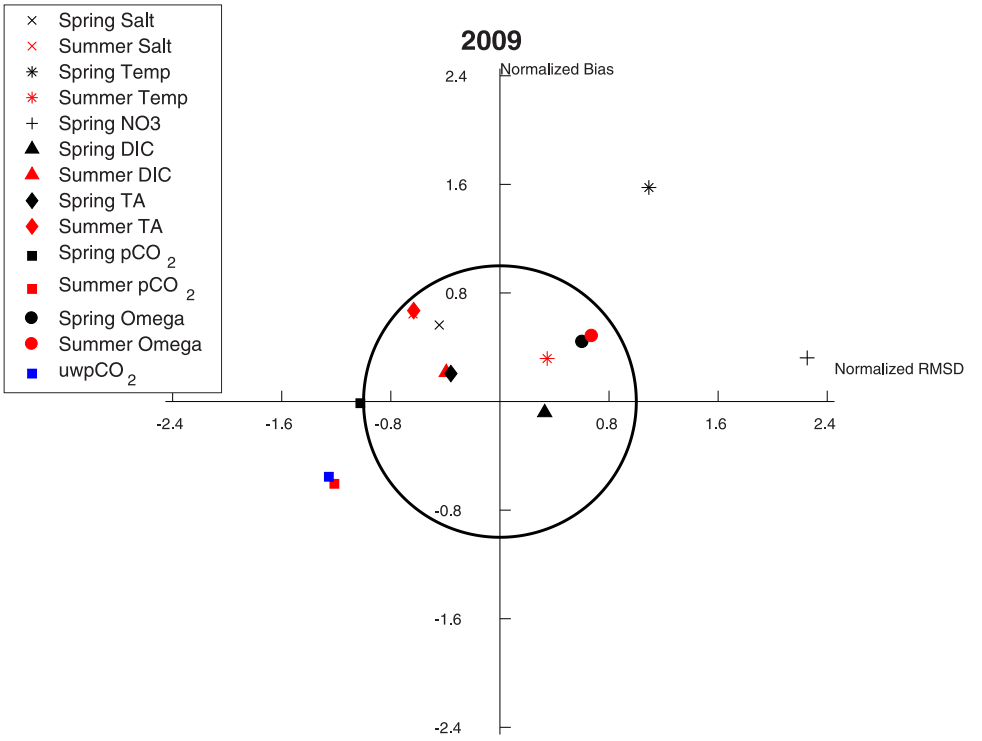

Figure 6. Target diagrams for model variables (salt = salinity, temp = temperature, NO3 = nitrate, Omega = aragonite saturation state) compared to observed data for all depths. Spring sampling points are colored in black while summer sampling points are colored in red. Comparisons are with the Seward Line data, except for the blue square, which uses Coastal uwpCO$_2$ data. The symbols show whether the model standard deviation (Normalized RMSD) is larger (X > 0) or smaller (X < 0) than the observations and whether the model has a positive (Y > 0) or negative (Y < 0) bias. A value within the black circle of one significantly simulates the variability in the observations.

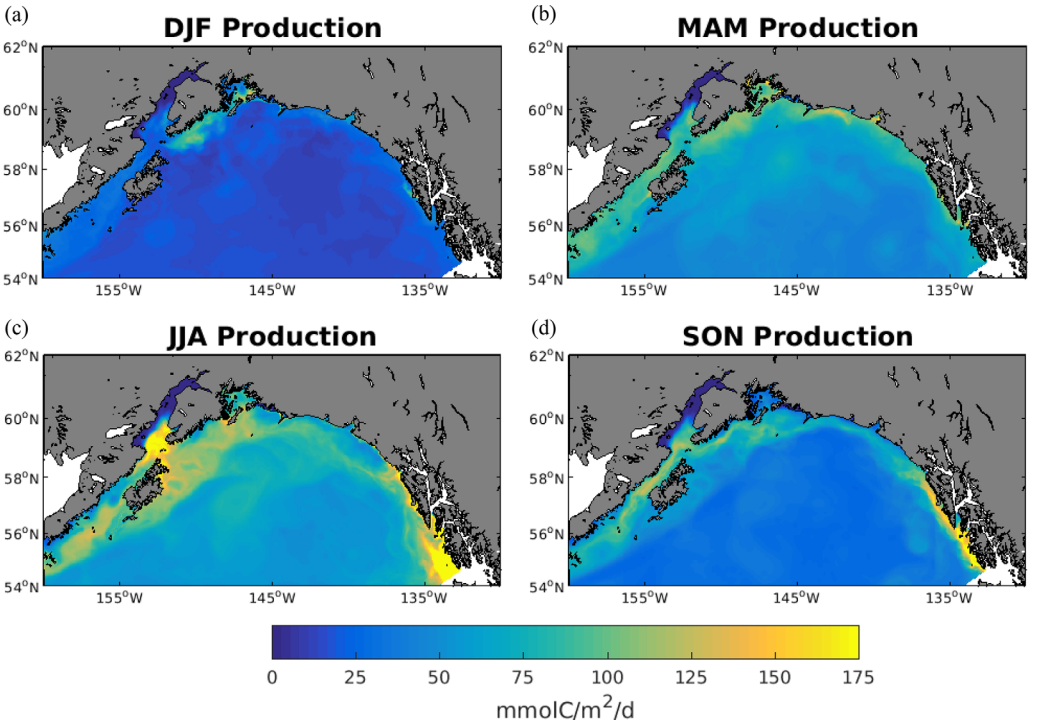

Figure 7. Seasonal mean maps of surface primary production integrated over the surface 200 m: (a) December–February (DJF), (b) March–May (MAM), (c) June–August (JJA), and (d) September–November (SON).

salinities as evident in Figure 5, an observation was made by Evans et al (2013, 2015). The regressions used in Evans et al. (2013) for DIC and TA ended up having different relationships to temperature and salinity for the region. Similarly, measurements above 33.6 salinity were deep samples collected over the outer continental shelf and have a steeper TA-salinity relationship (Evans et al., 2015). While the final regressions we used here had different salinity cutoffs that were associated with those outer continental shelf locations, the cutoff for DIC is not as distinct as TA. The cutoff could be closer to that of TA, and would require more analysis to better determine to come to any interesting conclusions. We chose this version as the regression fit slightly better.

Through initial model testing, we determined that model output TA and DIC were biased high due to a model salinity bias. This bias of up to 1–2 salinity units was described in Dobbins et al. (2009) and also by Stabeno et al. (2008) in a ROMS-based Bering Sea model. Because the TA and DIC boundary and initial conditions for the GOA model are derived from linear regressions with salinity, the model salinity bias produces subsequent biases in model output TA and DIC. To reduce this bias, we calculated a salinity offset used exclusively for generating the TA and DIC boundary and initial conditions. For this offset, we calculated the regression between model output salinity and observed salinity collected during the 2009 Coastal uwpCO$_2$ cruise conducted by the NOAA PMEL Coastal Carbon Dynamics and Ocean Acidification research programs (Figure 5). We used the following robust linear regression for salinity points that were greater than 31.9:

$$S = 1.6485 * S_0 - 22.2738 \quad (10)$$

where S is the bias corrected salinity value and S_0 is the initial salinity value. For salinity points less than 31.9, we simply reduced the salinity value by 1. This value was selected based on the analysis of Dobbins et al. (2009) and on a mean model bias of 1.1 for salinity less than 31.9 when compared with the Coastal uwpCO$_2$ cruise data. This method produced the best overall goodness of fit, compared to alternate methods of a single linear regression and a piecewise linear regression. The single linear regression significantly reduced the model bias at intermediate salinity levels (30–32 psu), but overcorrected at subsurface high salinity values, producing the undesirable effect of homogenizing salinity in the vertical. We also tested a piecewise linear regression, but this regression produced low R^2 values. To reiterate, the salinity offset does

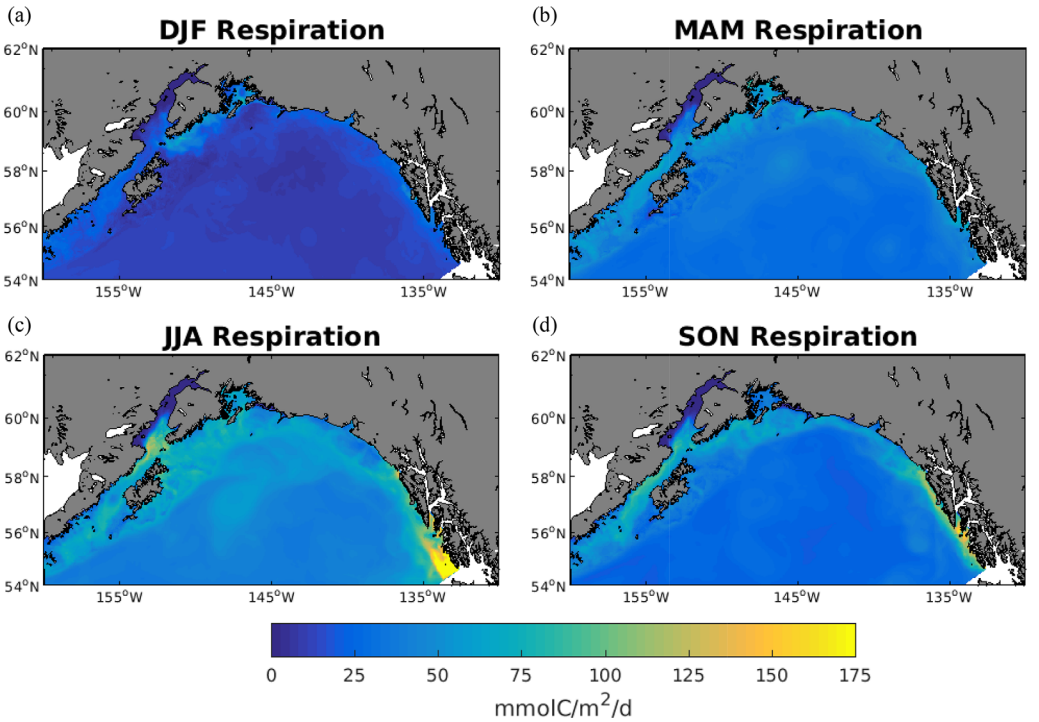

Figure 8. Seasonal mean maps of respiration (microbial and grazing) integrated over the surface 200 m: (a) December–February (DJF), (b) March–May (MAM), (c) June–August (JJA), and (d) September–November (SON).

not impact the modeled salinity or physical dynamics, only the boundary and initial conditions for the variables NO_3, DIC, and TA. We applied these relationships to generate the initial and boundary conditions of those variables for the GOA model, by first interpolating salinity fields from as predicted by the NEP model, subsequently applying the bias corrections, and finally calculating NO_3, DIC, and TA using (6)–(9). Initial conditions (at 1 January 2009), as well as boundary conditions for all other model variables, were interpolated from a long-term NEP hindcast simulation that began in year 1996 (Coyle et al., 2012; Hermann et al., 2009a).

2.5. Skill Assessment

Opportunistic sampling of the water column commenced along the Seward Line (Figure 1) in the 1970s, and temperature, salinity, nutrients, and plankton biomass have been systematically sampled at least twice a year since 1997. Additional observations for the carbon system were added in 2009 to the Seward Line, which we use as our primary observations for skill assessment. To quantify the overall correspondence between the observed and modeled fields, target diagrams (Jolliff et al., 2009) were made from profile observations and colocated model profiles in order to provide a summary of the pattern statistics and model biases for 2009 only. In target diagrams, the distance from the origin is proportional to the total root mean squared difference (RMSD). The target diagram indicates if the model's standard deviation is larger ($X > 0$) or smaller ($X < 0$) than the standard deviation of the observations in addition to providing information about the positive ($Y > 0$) or negative ($Y < 0$) bias. If modeled fields fall within values of 1 of the RMSD and bias, each normalized by the standard deviation of the observations, that indicates a better than average modeling efficiency metric (Stow et al., 2009) and that the observations and colocated modeled points are positively correlated (Jolliff et al., 2009).

2.6. Experiments

We conducted a sensitivity experiment using three model simulations that varied the value of alkalinity present in the freshwater forcing (Table 1). The model was run for 2009 and then the end of 2009 was used to initialize it again to have a full year of spin-up with carbon variables present prior to establishing a baseline state and perturbing the state with variable freshwater forcing. Each model simulation was started from an

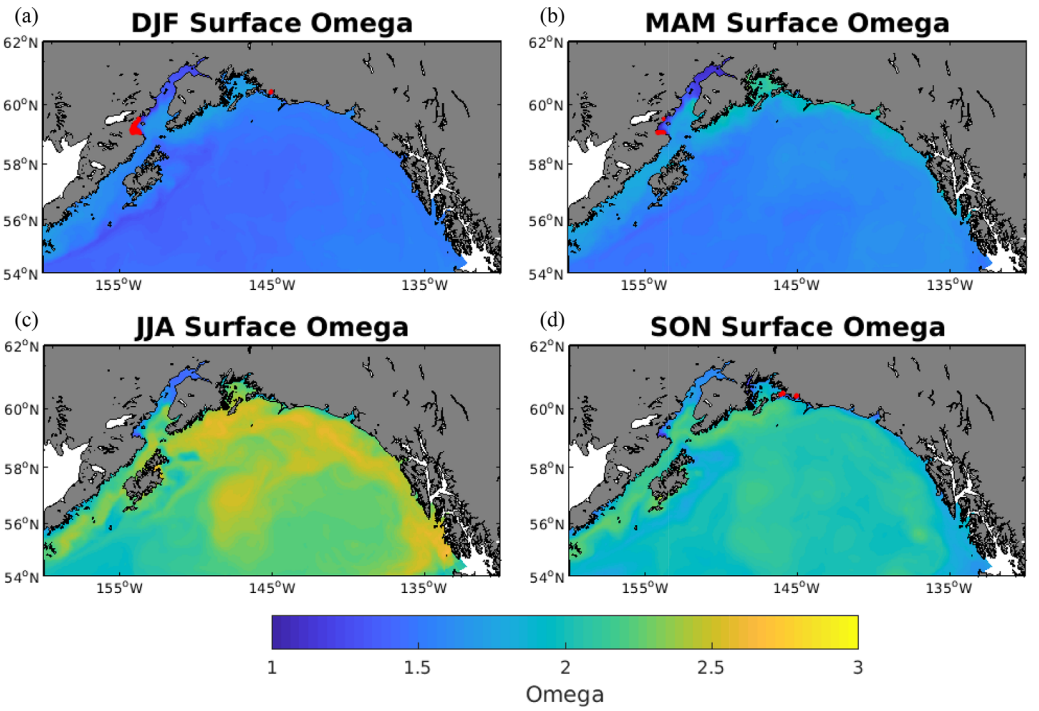

Figure 9. Seasonal mean maps of surface aragonite saturation state (Ω) for 2009 (a) December–February (DJF), (b) March–May (MAM), (c) June–August (JJA), and (d) September–November (SON). Red dots indicate undersaturated conditions ($\Omega < 1$).

identical spin-up state. The year 2009 was chosen as the study year due to the availability of high-resolution carbon chemistry data for model validation and existing physical simulations published elsewhere (Hermann et al., 2009b). The "low-alkalinity" scenario is calculated from the zero salinity end-member observed in river outflow to Prince William Sound (Evans et al., 2014) and is similar in magnitude to TA measured near tidewater-dominated glacial outflow (Alkire et al., 2015). This experiment is the "baseline" and considered the most representative of tidewater-dominated glacial outflow to the current GOA system. Two additional scenarios were tested with increased TA, which would happen with a transition from tidewater-dominated to proglacial-dominated freshwater runoff. There are currently no projections for the TA concentration in freshwater runoff in the Gulf of Alaska, so we select two values that are substantially greater than the current end-member estimate (Table 1). The range is still constrained by observed values from major river systems and glacially fed streams (Anderson et al., 2000; Cooper et al., 2008; Stets et al., 2014). The results of these experiments will help identify and quantify the importance of this climatically sensitive and relatively unconstrained regional forcing for Ω variability in the region.

3. Results

3.1. Model Performance

The model physical and biological variables have been validated in prior work (Coyle et al., 2012; Dobbins et al., 2009; Hermann et al., 2009b; Hinckley et al., 2009). As noted by Dobbins et al. (2009) and Stabeno et al. (2008), modeled salinity is biased high by 1–2 psu units in the basin, and is probably the result of the large-scale NEP model being too salty. The freshwater lens also does not penetrate as deep into the water column as observed (Dobbins et al., 2009), but the velocities and transport of the ACC compare well with observations. The biological model experiences higher than observed productivity in the shallow regions when compared to SEAWIFS, but it is able to simulate a low-nutrient, high-chlorophyll condition for coastal waters in summer, alongside a high-nutrient, low-chlorophyll condition for oceanic waters (Hinckley et al., 2009). The cross-shelf and vertical gradients and the seasonal cycle of chlorophyll and nutrients are well simulated by the model (Coyle et al., 2012) when compared to the Seward Line data sets from spring and fall of 2009 using the target diagram (Figure 6). All the modeled fields compare well with observations

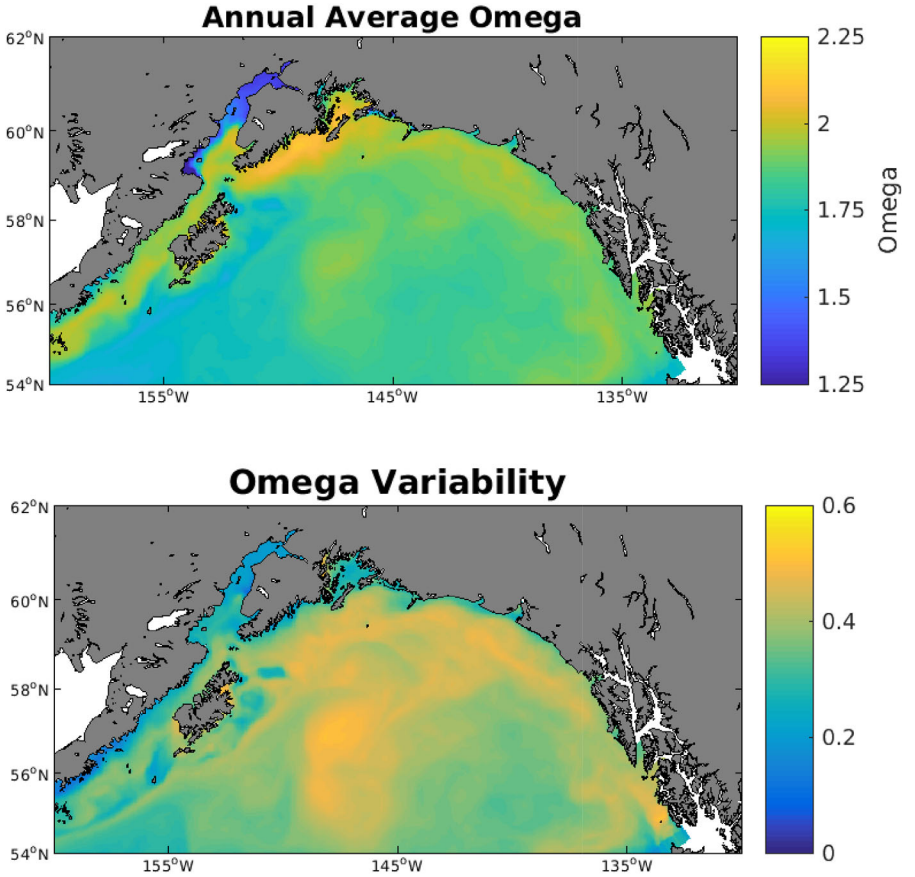

Figure 10. (a) Annual mean map of surface Ω for 2009. (b) Standard deviation of surface annual average Ω for 2009.

except for springtime temperature and nitrate. TA and DIC significantly simulate the spatial and temporal variability in that region of the GOA (within the value of 1 for normalized RMSD and bias on Figure 6). Spring temperature is biased high but significantly simulates the spatial and temporal variability in the region. Springtime nitrate is not biased, but simulates more variability in the region than is observed.

These biases and performance issues translate into the derived carbon variables, such as spring pCO_2. Figure 6 compares the observed Ω with the modeled values from the Seward Line for both spring and fall of 2009. Overall, the model has good agreement with the observed Ω (Figure 6). The model is biased high near the surface (not shown). This bias decreases with depth, and is nearly zero around the depths of the undersaturation horizon, which suggests that there is more uncertainty in the simulated conditions in the supersaturated range of Ω near the surface.

3.2. Seasonal Patterns

The seasonal cycle of 2009 is depicted in a series of seasonally averaged maps in Figures 7–9. Integrated water column production varies seasonally, and is highest in the summer months and lowest in the winter (Figure 7). Integrated water column respiration (including microbial, primary producers, and grazers) varies seasonally with productivity. Respiration in the model is highest in the summer months and lowest in the winter (Figure 8). The highest values of Ω occur in the summer (August) and the lowest values occur in the winter (Figure 9). In the fall months, there is more intense freshwater delivery to the region. Undersaturated conditions ($\Omega < 1$) are present in Cook Inlet in the fall and winter, highlighted by the red dots (Figure 9). This corresponds to a region of high freshwater input (Figure 3). While observations are limited in the Cook Inlet, a recent paper by Evans et al. (2013) from within Prince William Sound does suggest low Ω in that region, which is consistent with the model.

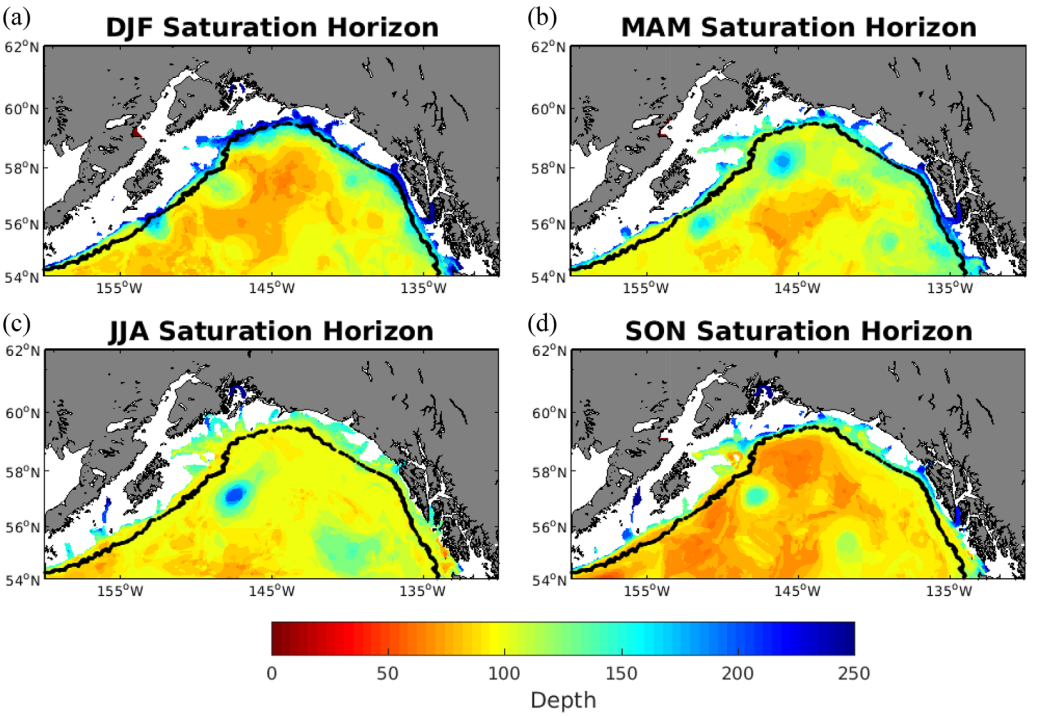

Figure 11. Depth of aragonite saturation horizon ($\Omega = 1$) seasonally averaged for the modeled region in 2009 for: (a) December–February (DJF), (b) March–May (MAM), (c) June–August (JJA), and (d) September–November (SON). Depth is reported in meters and only depicted for the upper 250 m. When the horizon is deeper, it is depicted in the same hue as 250. When the horizon is not present in the water column, the region is white. The black line indicates the 1500 m isobath.

The annual average surface Ω (Figure 10a) highlights some of the spatial variability in the region. First, a large (nearly an Ω difference of 1) east/west difference within the GOA exists with the highest values in the east, and the lowest values within Cook Inlet in the west. The largest monthly variability (standard deviation $\sim$0.5, Figure 10b), or monthly variability, exists in the eastern region of the gulf, which experiences more freshwater delivery and has the fewest comparable observations. The eastern GOA is also the region with the highest Ω near the surface in the summer (Figure 9).

The depth of the Ω saturation horizon, seasonally averaged, is shallowest in the fall, (September–November, Figure 11d) and deepest in the winter around the shelf break. In the gyre, the saturation horizon depth is deepest in the spring and summer. The shallowest locations tend to be in the western GOA and offshore, in the gyre. On average, the depth of undersaturation hovers around 100 m in the region, which agrees well with observations (Evans et al., 2013; Fabry et al., 2009). Some regions right along the coast also experience Ω undersaturation very close to the surface (Cook Inlet), and these regions are isolated from the deeper undersaturated offshore waters, implying a different mechanism driving that spatial trend.

3.3. Alkalinity in Freshwater Sensitivity Tests

Increasing the alkalinity in the freshwater runoff to simulate the transition in glacial contribution of the freshwater flux mostly impacted the regions closest to land, and surface Ω. Ω increased with increasing TA in the freshwater runoff (Figures 12, 13, and 14). The increase was nearly linear at 0.002 Ω per 100 μmol/kg increase in TA. The greatest change was in Prince William Sound and in the eastern portion of the GOA. The changes in surface Ω from the freshwater forcing experiments (see Table 1) were as large as the simulated seasonal variability in the eastern GOA. Within the eastern GOA region, areas that experience the biggest change from the freshwater alkalinity experiments are areas with low seasonal variability. The alkalinity from the freshwater forcing similarly increased seasonal variability in areas close to land and also in Prince William Sound and the eastern GOA (Figures 12, 13, and 14).

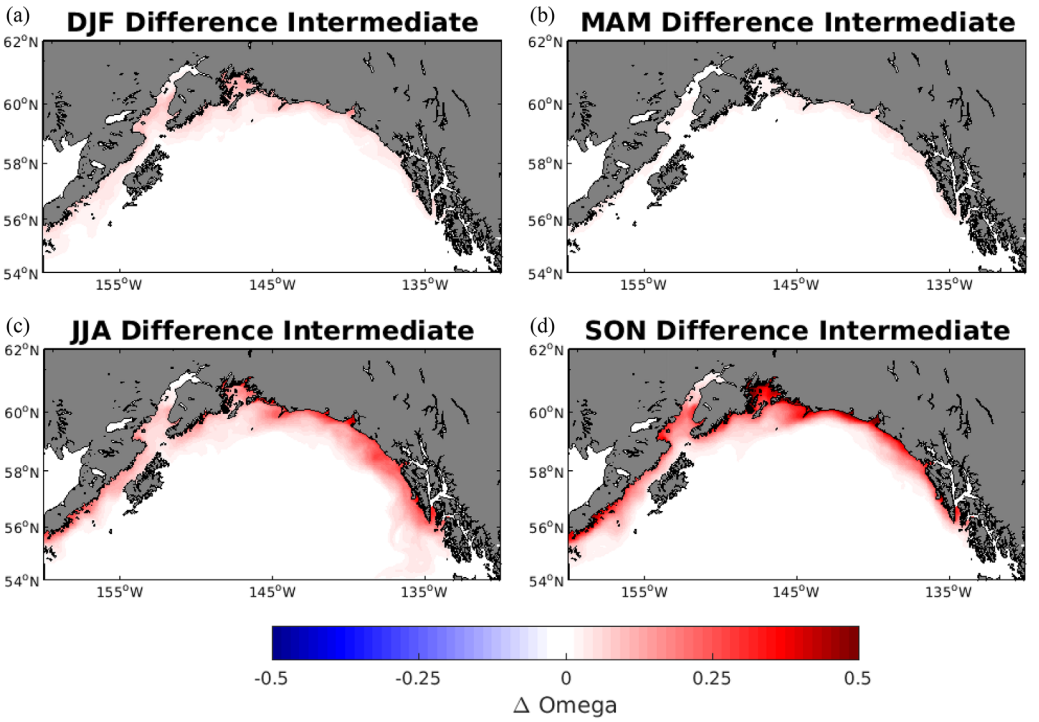

Figure 12. Difference plots between the "intermediate-alkalinity" scenarios and the "low-alkalinity" scenario in terms of surface Ω, where a positive value indicates an increase in compared to the "lowalkalinity" scenario for: (a) December–February (DJF), (b) March–May (MAM), (c) June–August (JJA), and (d) September–November (SON). Surface Ω is seasonally averaged.

3.4. Controls over Spatial Variability

Certain regions experience more respiration; in particular, the western GOA experiences more than the east, and the shallow regions next to the coast experience more than the deeper offshore waters (Figure 8). The balance between water column integrated respiration and production (hereafter referred to as local biological processes) influences the depth of Ω (Feely et al., 2016; Siedlecki et al., 2015). In addition to local biological processes, both winds and freshwater have been implicated in observational studies in the GOA as important for the location of the Ω depth horizon (Evans et al., 2014). In other regions, such as the California Current System, the depth of the aragonite saturation horizon has been shown to be spatially and temporally variable, with important influences from local biological processes and offshore upwelling (Feely et al., 2016).

Spatially, the patterns of local biological processes, freshwater, and winds are correlated with both the depth of the Ω horizon in the model and surface Ω in the model (Figures 15 and 16). For freshwater influences, salinity was used, with a *negative* correlation value indicating that deceased salinity yields a deeper horizon depth. For local biological processes, a *positive* correlation indicates that when production exceeds respiration there is and a deeper horizon depth. For the winds, a *negative* correlation indicates that a stronger NW (northwestward) wind stress yields a shallower horizon depth.

The Ω horizon depth is correlated with different processes in different areas of the GOA. Local biological processes dominate the western GOA offshore area with a *positive* correlation indicating that more production than respiration yields a deeper horizon depth. Along the shelf break, the western and eastern GOA Ω horizon depth is dominated by freshwater influences, while the central GOA shelf break area is correlated with local biological processes. The correlation between the freshwater influence and the depth of the Ω horizon is *positive*, indicating that under 2009 conditions, decreased salinity from runoff yields a shallower horizon depth.

Surface Ω variability is highly correlated to salinity and local biological processes throughout much of the region except for the nearshore regions on the central GOA shelf. The correlation between the freshwater influence and the surface Ω is *positive* within Cook Inlet, indicating decreased salinity yields a lower Ω. Offshore the correlation is *negative*, indicating increasing salinity yields a lower Ω. Local biological processes

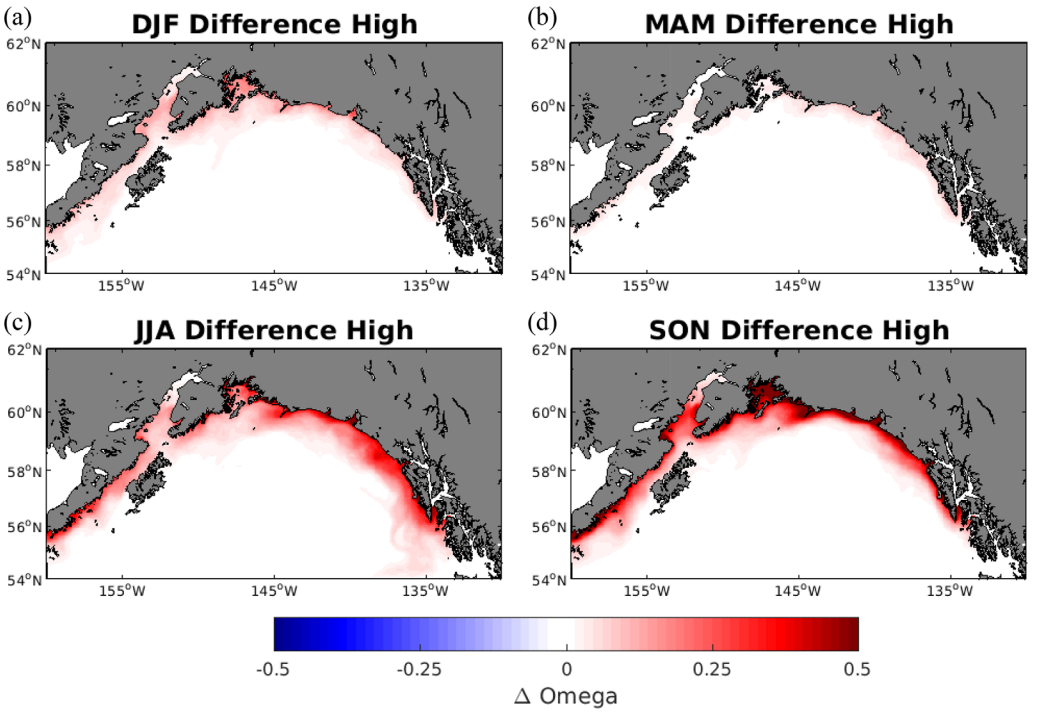

Figure 13. Difference plots between the "high-alkalinity" scenarios and the "low-alkalinity" scenario in terms of surface Ω, where a positive value indicates an increase compared to the "low-alkalinity" scenario for: (a) December–February (DJF), (b) March–May (MAM), (c) June–August (JJA), and (d) September–November (SON). Surface Ω is seasonally averaged.

dominate the western GOA region with a *positive* correlation indicating that more production than respiration yields a greater, less corrosive surface Ω. In the central GOA, a *negative* correlation indicates that a stronger SW (southwestward) wind stress yields a lower surface Ω.

4. Discussion

Observations and model results show that Ω varies spatially and temporally in the GOA. The proximity of low Ω waters at the surface to regional hatcheries, aquaculture, and sensitive rocky intertidal ecosystems is of interest to local stakeholders, tribes, and ecosystems. The shallow nature of the offshore saturation horizon, and its seasonal variability can cause habitat compression for benthic organisms (like crab) and pelagic organisms that are sensitive as well. Freshwater chemistry, local biological processes, and winds influence the modeled Ω fields. Freshwater brings a different water mass to the region, as described above, often less buffered in the GOA relative to the oceanic water, with its own distinct chemistry dependent on the contributions from glacial components. Local biological processes contribute in two ways—primary production draws carbon dioxide out of the atmosphere and into organic carbon, often increasing Ω. Respiration, conversely, returns organic carbon to carbon dioxide in the water column and consequently decreases Ω. The balance between these two processes determines the direction of the local biological process contributions to the spatial variability of Ω. Finally, winds contribute to the spatial variability of Ω in several ways. First, they bring deeper water to the surface through upwelling. Deeper waters have lower Ω. In the case of the GOA, stronger NW wind stress yields a shallower Ω horizon depth. Winds also advect waters with different signatures of Ω into a region, including freshwater. All of these processes contribute to the spatial variability in the region.

In the model, the depth horizon Ω is correlated spatially with respiration offshore, and salinity or local biological processes on the shelf (Figure 15). Surface Ω is spatially mostly positively correlated with salinity in nearshore waters along the western margin of the GOA and in Cook Inlet, inversely correlated with surface salinity offshore, and with local biological processes on the western shelf (Figure 16). The distinction

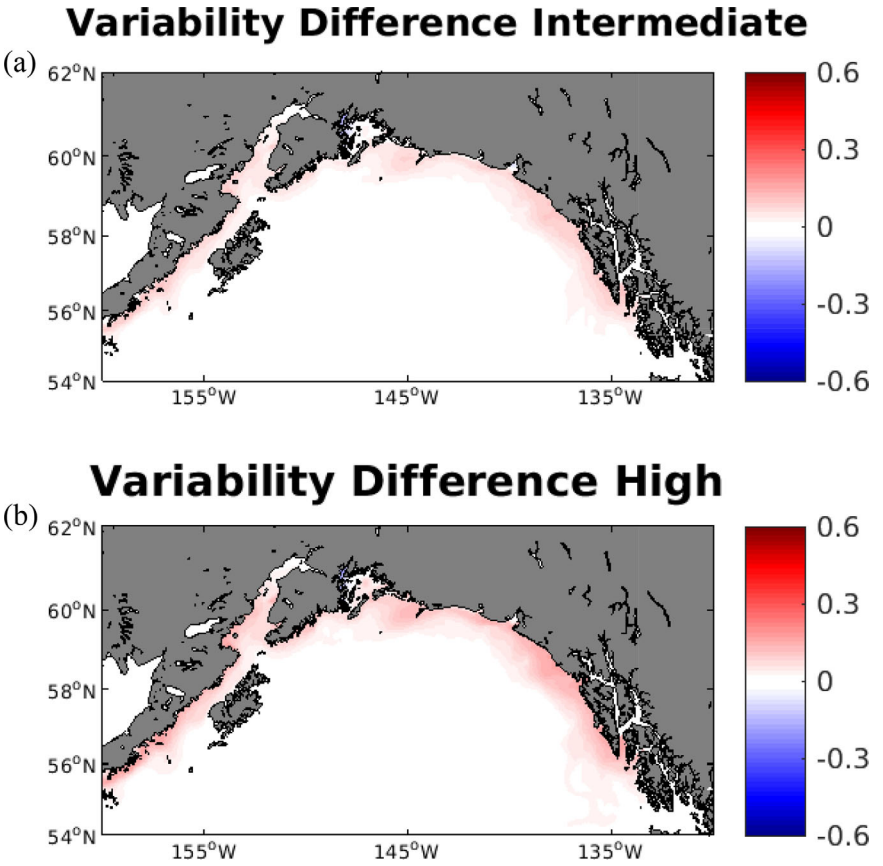

Figure 14. Difference plots between the (a) "intermediate" and (b) "high-alkalinity" scenarios and the "low-alkalinity" scenario in terms of the standard deviation of surface Ω over the year as an indication of variability, where a positive value indicates an increase in compared to the "low-alkalinity" scenario.

between the important processes nearshore and offshore—mostly in the direction of the correlations, highlight the important differences between these two environments.

On the shelf, the winds are most important in the nearshore regions, the alkalinity of the freshwater end-member is more important than offshore, and salinity has a different relationship in the correlations with Ω than it does offshore. The relative importance of each of these processes varies regionally. The strongest correlations in Figures 15 and 16 indicate that the winds experience the highest correlation (closest to 1) of any of the forcings with the annual pattern of Ω in the central GOA (SW winds) and the eastern GOA (NW winds). In the eastern GOA, this is interesting as the flux of freshwater is highest in the GOA in this region. The alkalinity end-member tests from this work showcased the sensitivity of the same nearshore region to the alkalinity of the freshwater entering the GOA, with impacts up to 0.5 units of Ω—nearly as much as the annual variability shown here (Figure 10b, 0.6 Ω units). This impact is largest in the fall (SON, Figures 12 and 13). The relationship between the lower salinity water and lower Ω is positive (Figure 16) in these nearshore regions, but reverses direction offshore in the deep basin of the GOA.

In the deep GOA, the Ω horizon depth is shallowest in the western part of the GOA in the fall (Figure 11). The correlation map (Figure 15) indicates this western region is most strongly correlated to the balance of biological processes in the region. This region could be dubbed a hot spot for Ω because of the persistence of shallow Ω depths throughout the simulation year. Regional hot spots for Ω are influenced by both local biological processes at depth and the relatively unconstrained chemistry of the freshwater delivery to the region at the surface. Interannually, the Ω in this offshore region will vary depending on the balance between production and respiration.

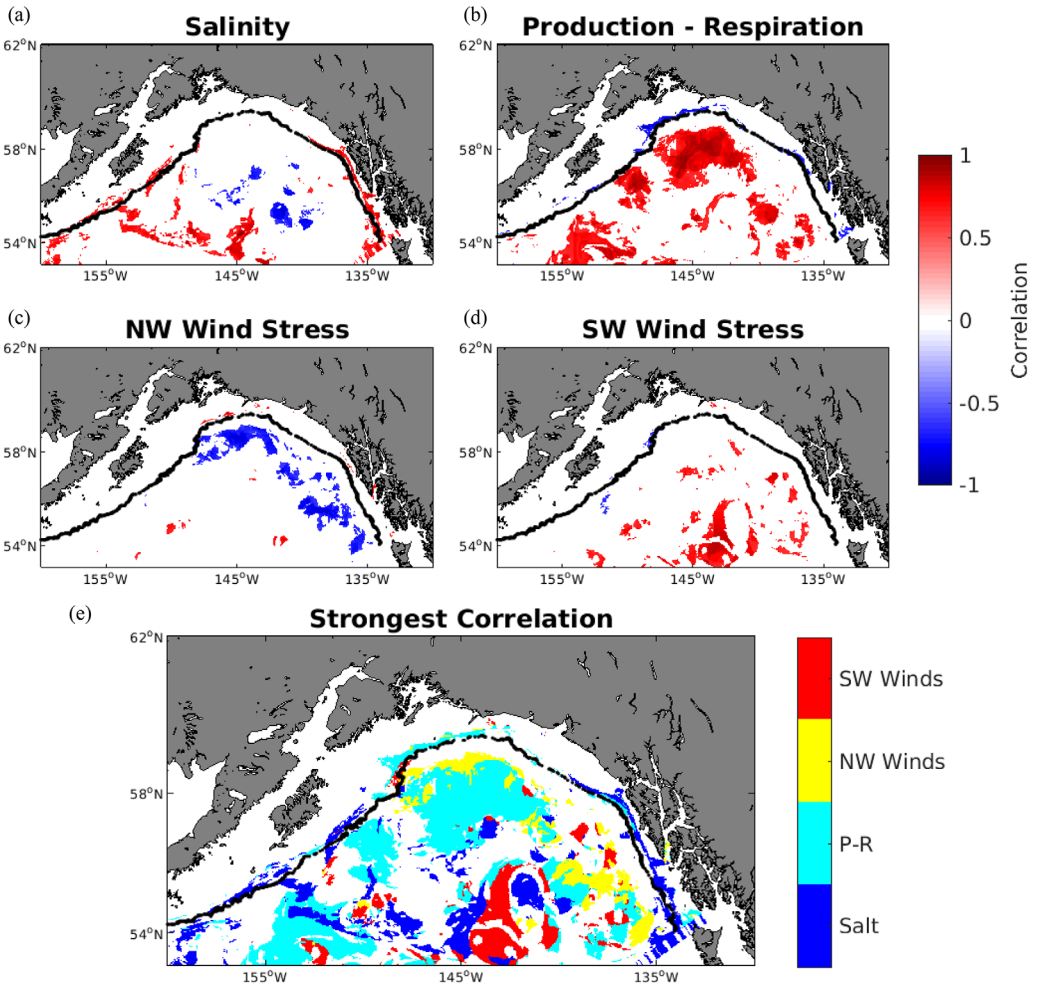

Figure 15. Spatial correlations at each model point between annual average aragonite saturation horizon depth and (a) surface salinity, (b) 0–200 m integrated production–respiration, (c) NW surface wind stress, (d) SW surface wind stress, and (e) the largest magnitude (positive or negative) correlation at each point. Only correlations with a magnitude greater than 0.6 and p-values less than 0.05 are shown. The black contour indicates the 1500 m isobath.

In the future, the peak freshwater forcing is expected to change with climate (Hill et al., 2015). An increase in fall discharge under RCP 8.5 conditions is expected along with a progression away from ice melt, toward more snowmelt and rain fall. Some of these changes should impact the OA-sensitive species in the GOA negatively, but the alkalinity is expected to rise with the changing source of the freshwater, consistent with the sensitivity experiment performed here, which would have an ameliorating effect. In addition, the timing of increased fall discharge could decrease the severity of ocean acidification events in the region. Fall is currently the time with the shallowest Ω horizon and largest area of undersaturated waters in the GOA.

Future projections using coarse global climate models indicate that SSTs will become warmer, with winter temperature anomalies exceeding 1.3°C by 2050 (Wang et al., 2010). Productivity is projected to decline over the next 100 years in the temperate North Pacific (Polovina et al., 2010), and the winds are projected to become more upwelling favorable at the coast, or a reduction in the magnitude of the downwelling-favorable winds (Yin, 2005). The reduction of productivity in the region should reduce the role of local biological processes on the Ω and further reduce the region's ability to uptake carbon. However, the productivity in these projections fails to include the potential increase in iron delivered to the GOA via glacial meltwater, which could increase productivity. The shoreward extent of the undersaturation horizon is thought to be driven by the annually integrated downwelling wind stress in the region (Evans et al., 2014),

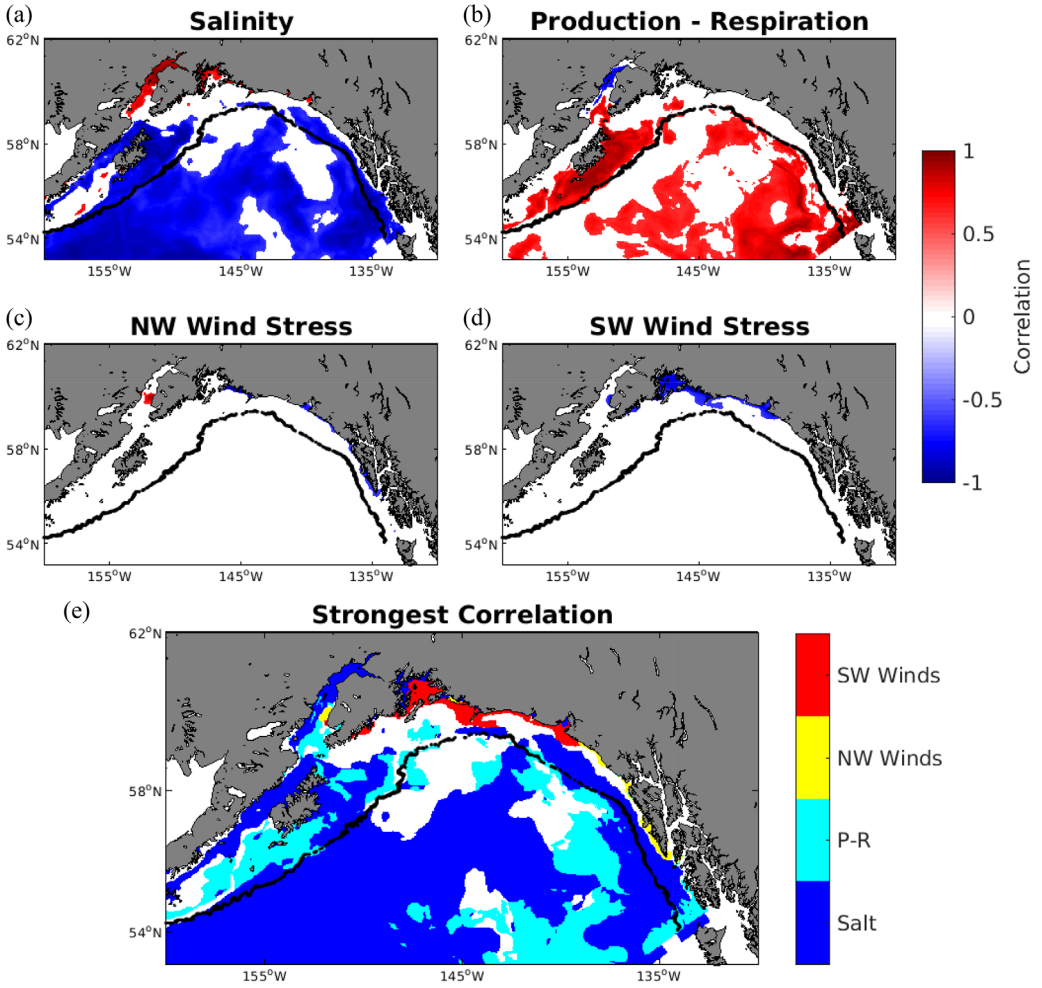

Figure 16. Spatial correlations at each model point between annual average surface aragonite saturation state and (a) surface salinity, (b) 0–200 m integrated production–respiration, (c) NW surface wind stress, (d) SW surface wind stress, and (e) the largest magnitude (positive or negative) correlation at each point. Only correlations with a magnitude greater than 0.6 and p-values less than 0.05 are shown. The black contour indicates the 1500 m isobath.

which would imply the shoaling of the saturation horizon everywhere in the GOA with the reduced downwelling wind stress in the future. The regions highlighted here as driven by wind stress are more susceptible to those projections than others. Our work here suggests that mostly the offshore regions will be influenced by the changes in the winds (at least for saturation depth), but a sensitivity study focused on the influence of the winds or a more extensive suite of hindcast experiments would be required to fully quantify the role of the winds. All of these processes are expected to change in different directions, making changes difficult to project without a fully coupled simulation.

5. Conclusions

We have presented results from a regional model with regional validation of physical, chemical, and biological constituents to separate the physical and biological variability contributing to the spatial variability of Ω in the GOA region in 2009. A regional data set has been used to constrain the model with sufficient skill to capture spatial patterns of Ω in the GOA coastal ocean. The model was added to an existing circulation and ecosystem model framework (Coyle et al., 2012; Hermann et al., 2009b). New model elements added to develop the Ω model include the coupling of ammonia cycling with inorganic carbon dynamics and freshwater forcing of the chemistry, both constrained by local observations.

Overall, the model results show that:

1. Freshwater forcing is important for the spatial distribution of surface Ω in nearshore regions populated with shellfish fisheries of the GOA.
2. The chemistry of that freshwater is not very well constrained, and is expected to change considerably in the future. This may as much as double the impact of the freshwater forcing on regional Ω variability.
3. Local winds, biological processes, and freshwater forcing all contribute to generating the spatial distribution of Ω in the GOA.
4. Local biological processes dominate the spatial variability controls of surface Ω in offshore waters of the region, while freshwater forcing dominates the nearshore waters.
5. The depth of the Ω horizon is correlated with local biological processes in the central GOA and the salinity forcing in the western and eastern GOA.

Results of the simulation of 2009 depicted the shallowest region for the saturation horizon in the western region of the GOA, but when broken down seasonally, the eastern GOA experienced the shallowest location in the summer months. Increasing the alkalinity of the freshwater end-member resulted in higher Ω values on the inner shelf.

Future work should focus on interannual variability in freshwater chemistry and discharge in combination, projecting these changes into the future, and identifying processes responsible for the spatial variability in retention. Understanding those processes is crucial to our ability to predict future trends in Ω in this region.

Appendix A

Equations for the carbon dynamics in the same manner as in Coyle et al. (2012) and the associated variables definitions in Tables A1 and A2 of that work. Note, advection and diffusion are omitted for simplicity in that work and consistently, in the equations below as well.

$$\begin{aligned}\frac{\partial DIC}{\partial t} = {} & \frac{degrad \cdot \mathrm{D}}{\xi} - \frac{\left[PS \cdot P_{MAX}\left(\tanh\left(\frac{\alpha \cdot PAR}{P^{*}_{\max}}\right)\right)\left(\frac{NO_3 e^{-\psi PS^{NH_4}}}{k_{1\ PS}+NO_3}\right)\left(\frac{Fe}{k_{fe\ PS}+Fe}\right)\left(\frac{k_{fe\ PS}+2}{2}\right)\right]}{12} \\ & - \frac{\left[PS \cdot P_{MAX}\left(\tanh\left(\frac{\alpha \cdot PAR}{P^{*}_{\max}}\right)\right)\left(\frac{NH_4}{k_{PS}+NH_4}\right)\left(\frac{Fe}{k_{fe\ PS}+Fe}\right)\left(\frac{k_{fe\ PS}+2}{2}\right)\right]}{12} \\ & - \frac{\left[PL \cdot P_{MAX}\left(\tanh\left(\frac{\alpha \cdot PAR}{P^{*}_{\max}}\right)\right)\left(\frac{NO_3 e^{-\psi PL^{NH_4}}}{k_{1\ PL}+NO_3}\right)\left(\frac{Fe}{k_{fe\ PL}+Fe}\right)\left(\frac{k_{fe\ PL}+2}{2}\right)\right]}{12} \\ & - \frac{\left[PL \cdot P_{MAX}\left(\tanh\left(\frac{\alpha \cdot PAR}{P^{*}_{\max}}\right)\left(\frac{k_{fe\ PL}+Fe}{Fe}\right)\right)\left(\frac{NH_4}{k_{PL}+NH_4}\right)\left(\frac{Fe}{k_{fe\ PL}+Fe}\right)\left(\frac{k_{fe\ PL}+2}{2}\right)\right]}{12} + \frac{R_{(i)}}{12} + E_{(i)}\end{aligned} \tag{A1}$$

$$\begin{aligned}\frac{\partial TA}{\partial t} = {} & degrad \cdot \mathrm{D} + \xi\left[PS \cdot P_{MAX}\left(\tanh\left(\frac{\alpha \cdot PAR}{P^{*}_{\max}}\right)\right)\left(\frac{NO_3 e^{-\psi PS^{NH_4}}}{k_{1\ PS}+NO_3}\right)\left(\frac{Fe}{k_{fe\ PS}+Fe}\right)\left(\frac{k_{fe\ PS}+2}{2}\right)\right] \\ & - \xi\left[PS \cdot P_{MAX}\left(\tanh\left(\frac{\alpha \cdot PAR}{P^{*}_{\max}}\right)\right)\left(\frac{NH_4}{k_{PS}+NH_4}\right)\left(\frac{Fe}{k_{fe\ PS}+Fe}\right)\left(\frac{k_{fe\ PS}+2}{2}\right)\right] \\ & + \xi\left[PL \cdot P_{MAX}\left(\tanh\left(\frac{\alpha \cdot PAR}{P^{*}_{\max}}\right)\right)\left(\frac{NO_3 e^{-\psi PL^{NH_4}}}{k_{1\ PL}+NO_3}\right)\left(\frac{Fe}{k_{fe\ PL}+Fe}\right)\left(\frac{k_{fe\ PL}+2}{2}\right)\right] \\ & - \xi\left[PL \cdot P_{MAX}\left(\tanh\left(\frac{\alpha \cdot PAR}{P^{*}_{\max}}\right)\left(\frac{k_{fe\ PL}+Fe}{Fe}\right)\right)\left(\frac{NH_4}{k_{PL}+NH_4}\right)\left(\frac{Fe}{k_{fe\ PL}+Fe}\right)\left(\frac{k_{fe\ PL}+2}{2}\right)\right] \\ & + \xi \cdot R_{(i)} + \xi \cdot E_{(i)} - 2 * nitr\end{aligned} \tag{A2}$$

Acknowledgments
Computations were done on the University of Washington Hyak supercomputer system, supported in part by the University of Washington eScience Institute. Regional U.S. IOOS, AOOS provided funding, and some of this work was leveraged from the NRC postdoctoral fellowship for D.P. Data were provided by multiple sources, including AOOS, the Seward Line, NOAA PMEL. NOAA data are available from CDIAC (http://cdiac.ornl.gov). Seward Line data are available from University of Alaska Fairbanks School of Fisheries & Ocean Sciences (https://www.sfos.uaf.edu/sewardline/). Monthly averaged model fields (T, S, Ω, NO_3, production, and respiration) are available in the University of Washington Libraries' ResearchWorks repository, using the following DOI: https://doi.org/10.6069/H5C82790. The authors would like to acknowledge the constructive reviews of two anonymous reviewers, which helped improve this manuscript. This publication is [partially] funded by the Joint Institute for the Study of the Atmosphere and Ocean (JISAO) under NOAA Cooperative Agreement NA10OAR4320148 (2010–2015) and NA15OAR4320063 (2015–2020), contribution 2017-069. This is PMEL contribution number 4619 and JISAO contribution number 2017-095.

References

Alkire, M. B., Nilsen, F., Falck, E., Søreide, J., & Gabrielsen, T. M. (2015). Tracing sources of freshwater contributions to first-year sea ice in Svalbard fjords. *Continental Shelf Research*, *101*, 85–97. https://doi.org/10.1016/j.csr.2015.04.003

Anderson, S. P., Drever, J. I., Frost, C. D., & Holden, P. (2000). Chemical weathering in the foreland of a retreating glacier. *Geochimica et Cosmochimica Acta*, *64*(7), 1173–1189.

Brewer, P. G., & Goldman, J. C. (1976). Alkalinity changes generated by phytoplankton growth. *Limnology and Oceanography*, *21*(1), 108–117. https://doi.org/10.4319/lo.1976.21.1.0108

Brickley, P. J., & Thomas, A. C. (2004). Satellite-measured seasonal and inter-annual chlorophyll variability in the Northeast Pacific and Coastal Gulf of Alaska. *Deep-Sea Research Part II: Topical Studies in Oceanography*, *51*, 229–245. https://doi.org/10.1016/j.dsr2.2003.06.003

Brown, G. H. (2002). Glacier meltwater hydrochemistry. *Applied Geochemistry*, *17*, 855–883.

Caldeira, K., & Wickett, M. E. (2003). Anthropogenic carbon and ocean pH. *Nature*, *425*, 365.

Caldeira, K., & Wickett, M. E. (2005). Ocean model predictions of chemistry changes from carbon dioxide emissions to the atmosphere and ocean. *Journal of Geophysical Research*, *110*, C09S04. https://doi.org/10.1029/2004JC002671

Cheng, W., Hermann, A. J., Coyle, K. O., Dobbins, E. L., Kachel, N. B., & Stabeno, P. J. (2012). Macro- and micro-nutrient flux to a highly productive submarine bank in the Gulf of Alaska: A model-based analysis of daily and interannual variability. *Progress in Oceanography*, *101*, 63–77. https://doi.org/10.1016/j.pocean.2012.01.001

Cooper, L. W., McClelland, J. W., Holmes, R. M., Raymond, P. A., Gibson, J. J., Guay, C. K., & Peterson, B. J. (2008). Flow-weighted values of runoff tracers (δ^{18}O, DOC, Ba, alkalinity) from the six largest Arctic rivers. *Geophysical Research Letters*, *35*, L18606. https://doi.org/10.1029/2008GL035007

Coyle, K. O., Cheng, W., Hinckley, S. L., Lessard, E. J., Whitledge, T., Hermann, A. J., & Hedstrom, K. (2012). Model and field observations of effects of circulation on the timing and magnitude of nitrate utilization and production on the northern Gulf of Alaska shelf. *Progress in Oceanography*, *103, 16–41*. https://doi.org/10.1016/j.pocean.2012.03.002

Coyle, K. O., Gibson, G. A., Hedstrom, K., Hermann, A. J., & Hopcroft, R. R. (2013). Zooplankton biomass, advection and production on the northern Gulf of Alaska shelf from simulations and field observations. *Journal of Marine Systems*, *128*, 185–207. https://doi.org/10.1016/j.jmarsys.2013.04.018

Curchitser, E. N., Haidvogel, D. B., Hermann, A. J., Dobbins, E. L., Powell, T. M., & Kaplan, A. (2005). Multi-scale modeling of the North Pacific Ocean: Assessment and analysis of simulated basin-scale variability (1996–2003). *Geophysical Research Letters*, *110*, C11021. https://doi.org/10.1029/2005JC002902

Dai, A., Qian, T., Trenberth, K. E., & Milliman, J. D. (2009). Changes in continental freshwater discharge from 1948 to 2004. *Journal of Climate*, *22*, 2773–2792. https://doi.org/10.1175/2008JCLI2592

Danielson, S. L., Curchitser, E. N., Hedstrom, K. S., Weingartner, T. J., & Stabeno, P. J. (2011). On ocean and sea ice modes of variability in the Bering Sea. *Journal of Geophysical Research*, *116*, C12034. https://doi.org/10.1029/2011JC007389

Devol, A. H., & Hedges, J. I. (2001). Organic matter and nutrients in the mainstem Amazon River. In M. E. McClain, R. L. Victoria, & J. E. Richey (Eds.), *The biogeochemistry of the Amazon Basin* (pp. 275–306). New York, NY: Oxford University Press.

Dobbins, E. L., Hermann, A. J., Stabeno, P., Bond, N. A., & Steed, R. C. (2009). Modeled transport of freshwater from a line-source in the coastal Gulf of Alaska. *Deep-Sea Research Part II: Topical Studies in Oceanography*, *56*, 2409–2426. https://doi.org/10.1016/j.dsr2.2009.02.004

Doney, S. C., Fabry, V. J., Feely, R. A., & Kleypas, J. A. (2009). Ocean acidification: The other CO_2 problem. *Annual Review of Marine Science*, *1*, 169–192. https://doi.org/10.1146/annurev.marine.010908.163834

Evans, W., Mathis, J. T., & Cross, J. N. (2014). Calcium carbonate corrosivity in an Alaskan inland sea. *Biogeosciences*, *11*, 365–379. https://doi.org/10.5194/bg-11-365-2014

Evans, W., Mathis, J. T., Ramsay, J., & Hetrick, J. (2015). On the frontline: Tracking ocean acidification in an Alaskan shellfish hatchery. *PLoS ONE*, *10*(7), e0130384. https://doi.org/10.1371/journal.pone.0130384

Evans, W., Mathis, J. T., Winsor, P., Statscewich, H., & Whitledge, T. E. (2013). A regression modeling approach for studying carbonate system variability in the northern Gulf of Alaska. *Journal of Geophysical Research: Oceans*, *118*, 476–489. https://doi.org/10.1029/2012JC008246

Fabry, V. J., McClintock, J. B., Mathis, J. T., & Grebmeier, J. M. (2009). Ocean acidification at high latitudes: The bellwether. *Oceanography*, *22*(4), 160–171.

Fabry, V. J., Seibel, B. A., Feely, R. A., & Orr, J. C. (2008). Impacts of ocean acidification on marine fauna and ecosystem processes. *ICES Journal of Marine Science*, *65*, 414–432. https://doi.org/10.1093/icesjms/fsn048

Feely, R. A., Alin, S. R., Carter, B., Bednaršek, N., Hales, B., Chan, F., . . . Juranek, L. (2016). Chemical and biological impacts of ocean acidification along the west coast of North America. *Estuarine, Coastal and Shelf Science*, *183*, 260–270. https://doi.org/10.1016/j.ecss.2016.08.043

Feely, R. A., Sabine, C. L., Lee, K., Barelson, W., Kleypas, J., Fabry, V. J., & Millero, F. J. (2004). Impact of anthropogenic CO_2 on the $CaCO_3$ system in the oceans. *Science*, *305*, 362–366. https://doi.org/10.1126/science.1097329

Fennel, K., Wilkin, J., Previdi, M., & Najjar, R. (2008). Denitrification effects on air-sea CO_2 flux in the coastal ocean: Simulations for the northwest North Atlantic. *Geophysical Research Letters*, *35*, L24608. https://doi.org/10.1029/2008GL036147

Fransson, A., Chierici, M., Nomura, D., Granskog, M. A., Kristiansen, S., Martma, T., & Nehrke, G. (2015). Effect of glacial drainage water on the CO_2 system and ocean acidification state in an Arctic tidewater-glacier fjord during two contrasting years. *Journal of Geophysical Research: Oceans*, *120*, 2413–2429. https://doi.org/10.1002/2014JC010320

Gay, S. M., III., & Vaughan, S. L. (2001). Seasonal hydrography and tidal currents of bays and fjords in Prince Williams Sound, Alaska. *Fisheries Oceanography*, *10*(1), 159–193. https://doi.org/10.1046/j.1054-6006.2001.00041.x

Goldman, J. C., & Brewer, P. G. (1980). Effect of nitrogen source and growth rate on phytoplankton-mediated changes in alkalinity. *Limnology and Oceanography*, *25*(2), 352–357.

Haidvogel, D. B., Arango, H., Budgell, W. P., Cornuelle, B. D., Curchitser, E., Di Lorenzo, E., . . . Wilkin, J. (2008). Ocean forecasting in terrain-following coordinates: Formulation and skill assessment of the Regional Ocean Modeling System. *Journal of Computational Physics*, *227*, 3595–3624. https://doi.org/10.1016/j.jcp.2007.06.016

Haines, J. R., Atlas, R. M., Griffiths, R. P., & Morita, R. Y. (1981). Denitrification and nitrogen fixation in Alaskan continental shelf sediments. *Applied and Environmental Microbiology*, *41*(2), 412–421.

Hermann, A. J., Curchitser, E. N., Haidvogel, D. B., & Dobbins, E. L. (2009a). A comparison of remote vs. local influence of El Niño on the coastal circulation of the northeast Pacific. *Deep-Sea Research Part II: Topical Studies in Oceanography*, *56*, 2427–2443. https://doi.org/10.1016/j.dsr2.2009.02.005

Hermann, A. J., Hinckley, S., Dobbins, E. L., Haidvogel, D. B., Bond, N. A., Mordy, C., . . . Stabeno, P. J. (2009b). Quantifying cross-shelf and vertical nutrient flux in the Coastal Gulf of Alaska with a spatially nested, coupled biophysical model. *Deep-Sea Research Part II: Topical Studies in Oceanography*, *56*, 2474–2486. https://doi.org/10.1016/j.dsr2.2009.02.008

Hermann, A. J., Ladd, C., Cheng, W., Curchitser, E. N., & Hedstrom, K. (2016). A model-based examination of multivariate physical modes in the Gulf of Alaska. *Deep Sea Research Part II: Topical Studies in Oceanography*, *132*, 68–89. https://doi.org/10.1016/j.dsr2.2016.04.005

Hill, D. F., Bruhis, N., Calos, S. E., Arendt, A., & Beamer, J. (2015). Spatial and temporal variability of freshwater discharge into the Gulf of Alaska. *Journal of Geophysical Research: Oceans*, *120*, 634–646. https://doi.org/10.1002/2014JC010395

Hinckley, S., Coyle, K. O., Gibson, G., Hermann, A. J., & Dobbins, E. L. (2009). A biophysical NPZ model with iron for the Gulf of Alaska: Reproducing the differences between an oceanic HNLC ecosystem and a classical northern temperature shelf ecosystem. *Deep-Sea Research Part II: Topical Studies in Oceanography*, *56*, 2520–2536. https://doi.org/10.1016/j.dsr2.2009.03.003

Jolliff, J. K., Kindle, J. C., Shulman, I., Penta, B., Friedrichs, M. A. M., Helber, R., & Arnone, R. A. (2009). Summary diagrams for coupled hydrodynamic-ecosystem model skill assessment. *Journal of Marine Systems*, *76*, 64–82. https://doi.org/10.1016/j.jmarsys.2008.05.014

Larsen, C. F., Burgess, E., Arendt, A. A., O'neel, S., Johnson, A. J., & Kienholz, C. (2015). Surface melt dominates Alaska glacier mass balance. *Geophysical Research Letters*, *42*, 5902–5908. https://doi.org/10.1002/2015GL064349

Mathis, J. T., Cooley, S. R., Lucey, N., Colt, S., Ekstrom, J., Hurst, T., . . . Feely, R. A. (2015). Ocean acidification risk assessment for Alaska's fishery sector. *Progress in Oceanography*, *136*, 71–91. https://doi.org/10.1016/j.pocean.2014.07.001

Napp, J. A., Incze, L. S., Ortner, P. B., Siefert, D. L. W., & Britt, L. (1996). The plankton of Shelikof Strait, Alaska: Standing stock, production, mesoscale variability and their relevance to larval fish survival. *Fisheries Oceanography*, *5*(1), 19–38. https://doi.org/10.1111/j.1365-2419.1996.tb00080.x

Neal, E. G., Hood, E., & Smikrud, K. (2010). Contribution of glacier runoff to freshwater discharge into the Gulf of Alaska. *Geophysical Research Letters*, *37*, L06404. https://doi.org/10.1029/2010GL042385

Niebauer, H. J., Royer, T. C., & Weingartner, T. J. (1994). Circulation of Prince William Sound, Alaska. *Journal of Geophysical Research*, *99*(C7), 14113–14126. https://doi.org/10.1029/94JC00712

Orr, J. C., Fabry, V. J., Aumont, O., Bopp, L., Doney, S. C., Feely, R. A., . . . Yool, A. (2005). Anthropogenic ocean acidification over the twenty-first century and its impact on calcifying organisms. *Nature*, *437*, 681–686. https://doi.org/10.1038/nature04095

Polovina, J. J., Dunne, J. P., Woodworth, P. A., & Howell, E. A. (2010). Projected expansion of the subtropical biome and contraction of the temperate and equatorial upwelling biomes in the North Pacific under global warming. *ICES Journal of Marine Science*, *68*, 986–995. https://doi.org/10.1093/icesjms/fsq198

Reisdorph, S. C., & Mathis, J. T. (2015). Assessing net community production in a glaciated Alaskan fjord. *Biogeosciences*, *12*, 5185–5198. https://doi.org/10.5194/bg-12-5185-2015

Royer, T. C. (1982). Coastal fresh water discharge in the northeast Pacific. *Journal of Geophysical Research*, *87*(C3), 2017–2021. https://doi.org/10.1029/JC087iC03p02017

Royer, T. C. (1998). Coastal processes in the northern North Pacific. In A. R. Robinson & K. H. Brink (Eds.), *The sea* (pp. 395–414). New York, NY: John Wiley.

Royer, T. C. (2005). Hydrographic responses at a coastal site in the northern Gulf of Alaska to seasonal and interannual forcing. *Deep-Sea Research Part II: Topical Studies in Oceanography*, *52*, 267–288. https://doi.org/10.1016/j.dsr2.2004.09.022

Royer, T. C., Vermersch, J. A., Weingartner, T. J., Niebauer, H. J., & Muench, R. D. (1990). Ocean circulation influencing the *Exxon Valdez* oil spill. *Oceanography*, *3*(2), 3–10. https://doi.org/10.5670/oceanog.1990.01

Sambrotto, R. N., & Lorenzen, C. J. (1987). Phytoplankton and primary production. In D. W. Hood & S. T. Zimmerman (Eds.), *The Gulf of Alaska: Physical environment and biological resources* (pp. 249–282). Silver Spring, MD: National Oceanic and Atmospheric Administration, U.S. Department of Commerce.

Sarmiento, J. L., & Gruber, N. (2006). *Ocean Biogeochemical Dynamics*. Princeton, NJ: Princeton University Press.

Schumacher, J. D., & Reed, R. K. (1980). Coastal flow in the northwest Gulf of Alaska: The Kenai Current. *Journal of Geophysical Research*, *85*(C11), 6680–6688. https://doi.org/10.1029/JC085iC11p06680

Shchepetkin, A. F., & McWilliams, J. C. (2005). The regional oceanic modeling system (ROMS): A split-explicit, free-surface, topography-following-coordinate oceanic model. *Ocean Modelling*, *9*, 347–404. https://doi.org/10.1016/j.ocemod.2004.08.002

Siedlecki, S. A., Banas, N. S., Davis, K. A., Giddings, S., Hickley, B. M., MacCready, P., . . . Geier, S. (2015). Seasonal and interannual oxygen variability on the Washington and Oregon continental shelves. *Journal of Geophysical Research: Oceans*, *120*, 608–633. https://doi.org/10.1002/2014JC010254

Stabeno, P. J., Bond, N. A., Hermann, A. J., Mordy, C. W., & Overland, J. E. (2004). Meteorology and oceanography of the northern Gulf of Alaska. *Continental Shelf Research*, *24*, 859–897.

Stabeno, P. J., Kachel, N., Mordy, C., Righi, D., & Salo, S. (2008). An examination of the physical variability around the Pribilof Islands in 2004. *Deep-Sea Research Part II: Topical Studies in Oceanography*, *55*, 1701–1716. https://doi.org/10.1016/j.dsr2.2008.03.006

Stabeno, P. J., Reed, R. K., & Napp, J. M. (2002). Transport through Unimak Pass, Alaska. *Deep-Sea Research Part II: Topical Studies in Oceanography*, *49*(26), 5931–5943.

Stets, E. G., Kelly, V. J., & Crawford, C. G. (2014). Long-term trends in alkalinity in large rivers of the conterminous US in relation to acidification, agriculture, and hydrologic modification. *Science of the Total Environment*, *488–489*, 280–289. https://doi.org/10.1016/j.scitotenv.2014.04.054

Stow, C. A., Jolliff, J., McGillicuddy, D. J., Doney, S. C., Allen, J. I., Friedrichs, M. A. M., . . . Wallhead, P. (2009). Skill assessment for coupled biological/physical models of marine systems. *Journal of Marine Systems*, *76*(1–2), 4–15. https://doi.org/10.1016/j.jmarsys.2008.03.011

Strom, S. L., Olson, M. B., Macri, E. L., & Mordy, C. W. (2006). Cross-shelf gradients in phytoplankton community structure, nutrient utilization, and growth rate in the coastal Gulf of Alaska. *Marine Ecology Progress Series*, *328*, 75–92. https://doi.org/10.3354/meps328075

Vaughan, S. L., Mooers, C. N. K., & Gay, S. M., III (2001). Physical variability in Prince William Sound during the SEA Study (1994–98). *Fisheries Oceanography*, *10*(1), 58–80. https://doi.org/10.1046/j.1054-6006.2001.0034.x

Wang, M., Overland, J. E., & Bond, N. A. (2010). Climate projections for selected large marine ecosystems. *Journal of Marine Systems*, *79*, 258–266. https://doi.org/10.1016/j.jmarsys.2008.11.028

Wanninkhof, R. (1992). Relationship between wind speed and gas exchange over the ocean. *Journal of Geophysical Research*, *97*, 7373–7382. https://doi.org/10.1029/92JC00188

Weingartner, T. J., Danielson, S. L., & Royer, T. C. (2005). Freshwater variability and predictability in the Alaska Coastal Current. *Deep-Sea Research Part II: Topical Studies in Oceanography*, *52*, 169–191. https://doi.org/10.1016/j.dsr2.2004.09.030

Weiss, R. (1974). Carbon dioxide in water and seawater: The solubility of a non-ideal gas. *Marine Chemistry*, *2*(3), 203–215.

Wu, J., Aguilar-Islas, A., Rember, R., Weingartner, T., Danielson, S., & Whitledge, T. (2009). Size-fractionated iron distribution on the northern Gulf of Alaska. *Geophysical Research Letters*, *36*, L11606. https://doi.org/10.1029/2009GL038304

Yin, J. H. (2005). A consistent poleward shift of the storm tracks in simulations of 21st century climate. *Geophysical Research Letters*, *32*, L18701. https://doi.org/10.1029/2005GL023684

Zeebe, R., & Wolf-Gladrow, D. (2001). *CO2 in seawater: Equilibrium, kinetics, isotopes, Elsevier Oceanography Series* (Vol. 65). Amsterdam, the Netherlands: Elsevier.